JOURNAL OF LOW DIMENSIONAL SYSTEMS
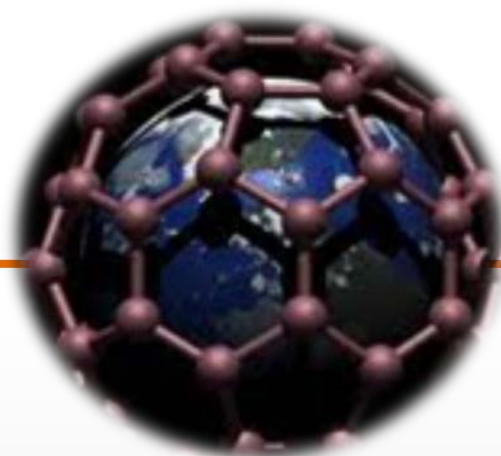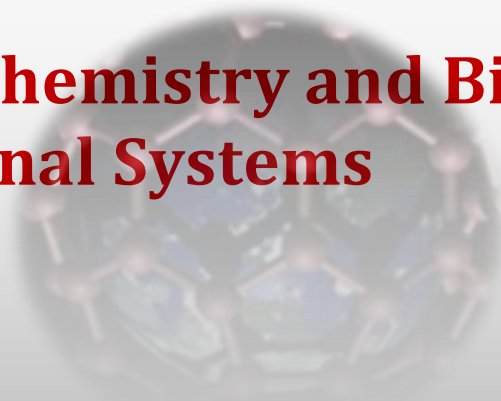
Physics, Chemistry and Biology of Low Dimensional Systems

Aims and scope

The *Journal of Low Dimensional Systems* is co-edited by Baku State University.

It publishes papers and review articles on the fundamental and applied aspects of physics, chemistry and biology. General areas of interest are the electronic, spectroscopic and structural properties of low dimensional systems, including perfect and defect lattices, surfaces, two-dimensional electron systems, interfaces, thin films and multilayers, amorphous materials, micro- and nanostructures, and layered structures. Papers dealing with biomaterials for medical purposes are accepted.

Typical examples include the preparation and structural characterization of novel and advanced low dimensional materials, especially in relation to the measurement and interpretation of their electrical, magnetic, optical, thermal and mechanical properties, phase transitions, electronic structure and defect properties, and the application of appropriate experimental and theoretical techniques in these studies. Articles are encouraged in all the above areas, but especially those which emphasize fundamental aspects of materials science.

Address:

Az1148, Z.Khalilov str. 23,
Baku State University, BSU publication, Baku, Azerbaijan

E-mail: mhhuseyng@bsu.edu.az

Journal of LDS

Table of Contents

STRUCTURAL AND OPTICAL CHARACTERIZATION OF COBALT OXIDE SYNTHESIZED BY SONOCHEMICAL METHOD

S.J.MAMMADYAROVA[1*], M.B.MURADOV[1], A.M.MAHARRAMOV[2], G.M.EYVAZOVA[1], Z.A.AGHAMALIYEV[1], O.O.BALAYEVA[2]

[1]Department of Physics, Baku State University, Z.Khalilov str.,23, AZ-1148 Baku, Azerbaijan
[2]Department of Chemistry, Baku State University, Z.Khalilov str.,23, AZ-1148 Baku, Azerbaijan

Cobalt oxide nanoparticles were synthesized by sonochemical reduction method using cobalt nitrate [$Co(NO_3)_2 \cdot 7H_2O$] and sodium borohydride ($NaBH_4$) as precursors and poly (vinyl) alcohol (PVA) as capping agent. Reaction was also carried out in ozone flow to investigate its effect on the optical and structural properties of the obtained cobalt oxide particles. The synthesized particles were characterized by UV-visible spectroscopy (UV-Vis), Fourier transform infrared (FT-IR) spectroscopy, X-ray diffraction (XRD), and energy dispersive X-ray analysis (EDAX).

1. INTRODUCTION

In recent years, among the transition metal oxides cobalt oxides have attracted considerable interest due to their optical, magnetic, catalytic and electronic properties. Cobalt has two stable oxides: CoO and Co_3O_4. CoO crystals adopt the rock salt structure and it has many applications based on magnetic [1], catalytic [2], and gas-sensing properties [3]. It is also widely used in the ceramics industry as an additive to create blue colored glazes and enamels. It is difficult to synthesize CoO nanoparticles in pure form, because in most cases the synthesized product consists of a mixture of Co metal or Co_3O_4. Various methods have been reported to synthesize CoO and Co_3O_4 nanoparticles with different morphologies such as solvothermal [4], spray roasting method [5], sol-gel [6], thermal decomposition [7], chemical bath deposition[8], solution combustion synthesis method [9], hydrothermal [10], chemical precipitation [11], sonochemical [12], pyrolysis [13], microwave-assisted [14] and electrospinning technique [15]. S. Chattopadhyay et al. [16] synthesized phosphonomethyliminodiacetic acid (PMIDA) coated CoO nanoparticle by thermal decomposition method and studied anti-cancer activity to cancer cell in vitro. 3D porous Co/CoO composite films have been prepared by electrodeposition method and was applied as cathode for alkaline hybrid batteries [17]. Co_3O_4 is a p-type antiferromagnetic oxide semiconductor. It is a mixed valence compound ($CoO \cdot Co_2O_3$) and adopts the normal spinel crystal structure, in which Co^{2+}ions occupy the tetrahedral 8a sites and Co^{3+}ions occupy the octahedral 16d sites. Co_3O_4 nanoparticles have potential applications such as supercapacitor [18], anode material in Li-ion batteries [19], gas sensors [20], catalysts [21], electrochemical sensor [22], solar absorbing material [23], electrochromic devices [24] etc.

In the present paper cobalt oxide nanoparticles were synthesized by sonochemical method. Firstly, cobalt nanoparticles were obtained by reducing with $NaBH_4$ and then subjected to oxidation with ozone. To the best of our knowledge, use of PVA as a stabilizing/capping agent was reported for the first time on the Co^{2+}-$NaBH_4$ redox reaction. The powders were characterized by XRD, UV-Vis and FT-IR spectroscopy and EDX analysis.

2. EXPERIMENTAL

For the preparation of nanostructured cobalt oxide, cobalt nitrate [$Co(NO_3)_2 \cdot 7H_2O$], sodium borohydride ($NaBH_4$) were used as pecursors and poly (vinyl) alcohol (PVA) was used as capping agent/stabilizer. For the synthesis, 0.1 M of $Co(NO_3)_2 \cdot 7H_2O$ was completely dissolved in 40 ml of distilled water. PVA solution (2.0 wt%) was prepared by dissolving the required amounts in the distilled water. As-prepared $NaBH_4$ (0.2 M) was added drop wise into the cobalt nitrate solution containing PVA under sonication process using an ultrasonic probe. This reaction was

sonicated for 1 h. The reaction of cobalt nitrate with poly (vinyl) alcohol followed by reduction with sodium borohydride leading to green powders. The obtained product was washed three times with deionized water and ethanol and collected through centrifugation. Finally, the synthesized sample was dried at room temperature. Similarly, the experiment was repeated by ozon flow, maintaining other reaction parameters. Finally, to achieve Co_3O_4 nanoparticles synthesized powders were annealed at 500ºC in air for 4 h. The reduction reaction between $Co(NO_3)_2 \cdot 7H_2O$ and $NaBH_4$ has been shown in the following equation:

$$Co(NO_3)_2 + 2NaBH_4 \rightarrow Co + 2NaNO_3 + B_2H_6 + H_2 \uparrow$$

The structural analysis of the synthesized oxide powders was analyzed by Rigaku Mini Flex 600 X-ray diffractometer (λ= 1.54060 Å) using Ni-filtered Cu Ka radiation. Optical properties of the samples were investigated by Specord 250 Plus UV-vis Spectrophotometer. FTIR measurement has been conducted within 400-4000 cm^{-1} region on a Varian 3600 FTIR spectrometer.

3. RESULTSAND DISCUSSION

The XRD patterns of nanoparticles are shown in Fig. 1. In the XRD pattern of samples synthesized in without [Fig.(a)-1] and under ozone flow condition [Fig.(b)-1] no peaks corresponding to cobalt or cobalt oxide were observed. It means that the prepared product consists of particles with amorphous nature. But after thermal annealing of powders at 500ºC in air for 4 h very small intensity peaks were appeared. For samples synthesized in without ozone reaction condition the diffraction peaks at 2θ values of 36.71º, 39.71º and 54.56º corresponding to (311), (222), (422) planes indicates the formation of low crystalline Co_3O_4 (JCPDS, card no 09-0418). The peak was also observed at 2θ=33.22º corresponding to (111) plane, which is in good agreement with CoO (JCPDS, card no 42-1300). It means that the obtained particles consist of two phases. For samples synthesized by the reaction with ozone flow the peaks were observed at 2θ values of 36.64º, 44.77º and 65.26º corresponding to (311), (400), (440) planes, indicate the formation of Co_3O_4. The existence of very small intensity peaks can be attributed small sized particles. The particle size

D of Co_3O_4 was calculated using the Scherrer formula:

$$D = 0.89\lambda/\beta\cos\theta \quad (1)$$
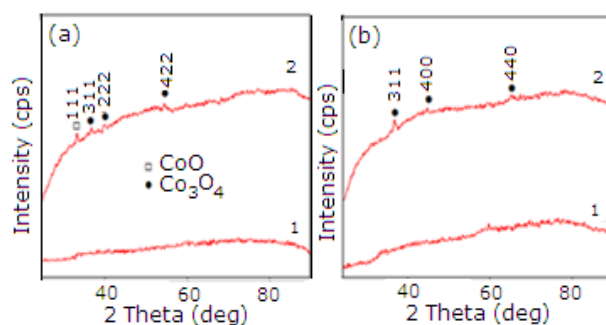
Figure 1.X-ray diffraction pattern of nanoparticles before (1) and after annealing (2) synthesized in (a) without ozone and (b) under ozone flow reaction condition

Evaluated from Eq. (1), the average size of Co_3O_4 particles obtained in ozone flow reaction condition is 14 nm. After annealing of samples synthesized in air in the diffractogram the intense peak corresponds to CoO for particles synthesized in normal reaction condition and particle size is 36 nm.

UV–vis spectra measurement was carried out to determine optical absorption properties of samples. The optical band gap (E_g) of the particles can be calculated using the following equation:

$$\alpha = B(h\nu - E_g)^n/h\nu \quad (2)$$

whereα is the absorption coefficient, $h\nu$ is the photonenergy, B is a constant, and the value of n is depend on nature of transition; ½for directly allowed and 2 for indirectly allowed transitions.
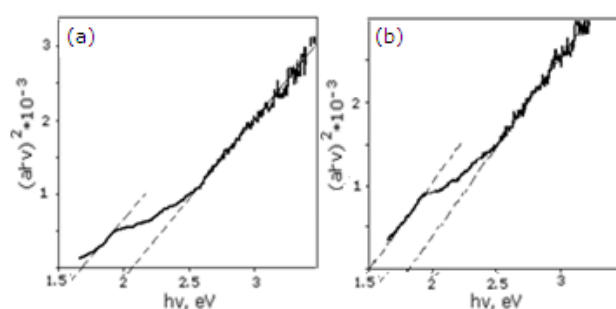
Figure 2.$(\alpha h\nu)^2$ versus $(h\nu)$ for Co_xO_y samples synthesized in a) without ozone and b) under ozone flow reaction condition

As shown in Fig. 2, Co_xO_y samples have two band gaps. The optical band gaps of samples before annealing obtained without and with ozone flow reaction condition are 1.65eV and 2.06 eV, 1.51eV

and 1.81 eV, respectively. The band gap energy decreases for samples synthesized in ozone flow reaction condition. It can be attributed that when nanoparticle interact with ozone their size gradually increase. Fig. 3 shows the band gap energies of particles after thermal annealing at 500°C in air. For samples obtained without and with ozone flow reaction condition band gap energy was calculated as 1.12 eV and 1.38 eV; 1.10 eVand 1.32 eV, respectively.
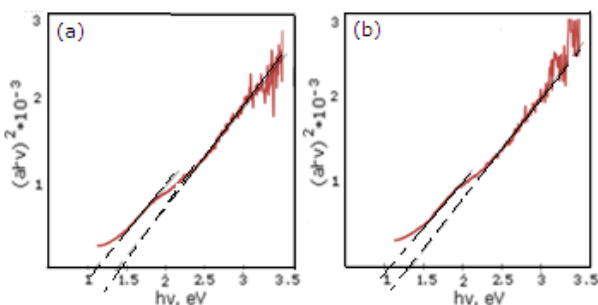
Figure 3.$(\alpha h\nu)^2$ versus (hν) for Co$_3$O$_4$ samples synthesized in a) without ozone and b) under ozone flow reaction condition

Fig. 4 and Fig. 5 show the IR spectrums of samples before and after annealing at 500°C. The strong and wide band at 3440 cm^{-1} and 3441 cm^{-1} observed at the spectra of particles synthesized in without and under ozone flow condition, respectively are attributed to the stretching vibrational mode of hydrogen bonded hydroxyl group of PVA. The absorption band at 2928 cm^{-1} for Co$_x$O$_y$ particles synthesized in without ozone and the band at 2920 cm^{-1} for particles synthesized in ozone flow condition are assigned to the asymmetric C-H stretching. Also, the band observed at 2851 cm^{-1} for ozone reaction is attributed to the symmetric C-H stretching [25]. The bending and wagging vibrations of CH$_2$ are found at 1443cm^{-1} and 1340 cm^{-1}, respectively. The bands at 1740 cm^{-1} (for without ozone reaction) and 1642 cm^{-1}(for ozone reaction) are assigned to the C=O stretching of the acetate group of PVA [26]. The band observed at 1126 cm^{-1} (for without ozone reaction) is the characteristic to the C–O stretching vibration. This characteristic peak was observed at 1121 cm^{-1} for ozone reaction and intensity of this peak decreased slightly. It can be due to the more nanoparticle formation and defects induced by them. Moreover, the absorbtion bands observed at 676 cm^{-1} and 655 cm^{-1} for without and with ozone flow

reaction condition, respectively, is assigned to the stretching vibration mode of metal-oxygen [14].

If we compare two spectrums, we can observe shift in the low frequency of peaks for ozone reaction. It can be explained by the fact that nanoparticle size was increased in ozon flow reaction due to the oxidation and obtained nanoparticles weakened of the chemical chain energy.
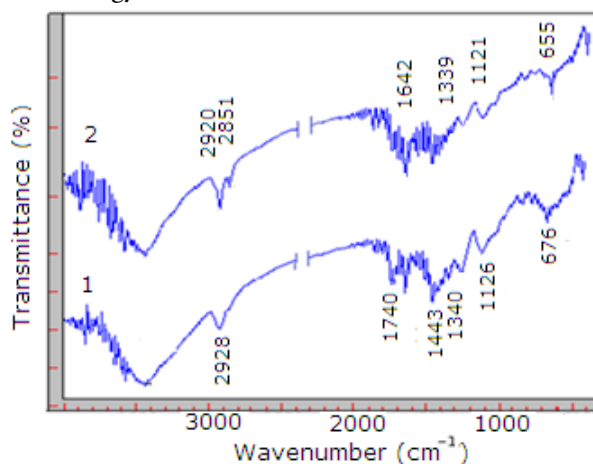

Figure 4.FT-IR spectrum of the powders before annealing synthesized in without ozone (1) and under ozone flow reaction condition (2)
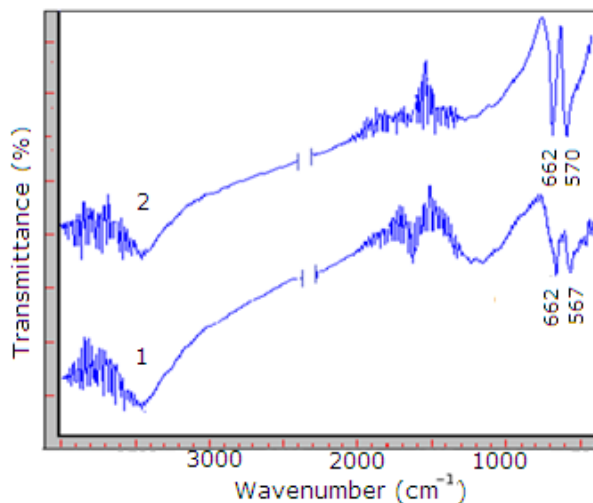
Figure 5. FT-IR spectrum of the Co$_3$O$_4$ powders synthesized in without ozone (1) and under ozone flow reaction condition (2)

After thermal annealing at 500°C of samples, two strongest and sharp peaks at 662 (ν_1) cm^{-1} and 567(ν_2) cm^{-1} for without ozone reaction, 662 ($\nu_{1'}$)cm^{-1} and 570 ($\nu_{2'}$)cm^{-1} for ozone flow reaction condition were observed. The ν_1 and $\nu_{1'}$ bands are attributed to the tetrahedral coordinated Co^{2+} ions, while the ν_2 and

$\nu_{2'}$bands is the characteristic to the octahedral coordinated Co^{3+} ions [27].
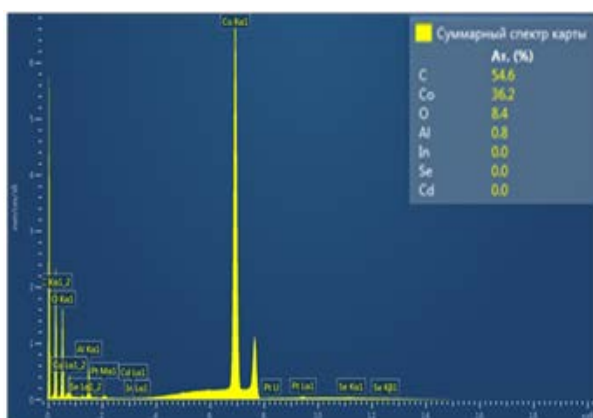
Figure 6.EDX spectrum of samples before annealing synthesized in without ozone reaction condition

These characteristic peaks are more intensive for ozone reaction. This may be due to more crystallinity of the particles. It is determined that bands of PVA have been disappeared after annealing at 500ºC. It indicates the decomposition and evaporation of PVA from nanocomposite [28].

Energy dispersive X-ray spectrometry (EDX) analysis was employed to determine the composition of the samples. EDX spectrum of particles before annealing synthesized without ozone reaction condition shows that the experimental atomic percentages of cobalt and oxygen are found to be 36.2% and 8.4%, respectively (Fig. 6).

This result indicates that the synthesized product consists mainly of cobalt nanoparticles and poor oxidation was occurred due to dissolved oxygen in the solution. For samples before annealing synthesized in ozone flow experimental atomic percentages of cobalt and oxygen are found to be 5.3% and 42.1%, respectively (Fig. 7). It is known that ozone is a strong oxidizer due to the formation of free oxygen radicals during decomposition and it has an active interaction with substances. For this reason strong oxidation of particles was occurred.
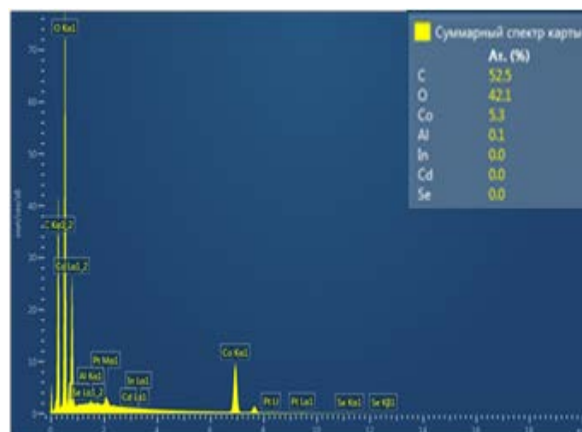
Figure 7.EDX spectrum of samples before annealing synthesized in ozone flow reaction condition

4. CONCLUSION

In the present study, we synthesized cobalt oxide nanoparticles by sonochemical reduction method using PVA as capping agent. It is observed two band gaps from optical studies for cobalt oxide. For samples after annealing obtained without and with ozone flow reaction condition band gap energy was calculated as 1.12 and 1.38 eV; 1.10 and 1.32 eV, respectively The band gap decreased for samples synthesized by ozon flow reaction. So it can be concluded that when nanoparticle interact with ozone, which is bubbled through a solution, the nanoparticles size gradually increase due to their losing aggregation stability.The average size of Co_3O_4 particles obtained in the reaction condition by ozon flow is calculated as 14 nm from XRD. FT-IR measurements also confirm the formation of Co_3O_4.

5. REFERENCES

1. Skumryev V.; Stoyanov S.; Zhang Y. et al. / Beating TheSuperparamagnetic Limit with Exchange Bias. Nature, 2003, v.423, p.850−853
2. Lin H. K.; Chiu H. C.; Tsai H. C. et al. / Catal. Lett., 2003, v.88, p.169−174.
3. Koshizaki. N.; Yasumoto.K.; Sasaki. T. / Sens. Actuators B, 2000, v.66, p.122−124
4. Lingna S., Huifeng L., Ling R., et al. /Solid State Sciences, 2009, v.11, p.108-112
5. Qiusong G., Xueyi G., Qinghua T. / Advanced Powder Technology, 2010, v.21, p. 529-533
6. Manoj P, Zahira Y. / Chemical Papers, 2014, v.68, p.1087−1096

7

7. Chen Z, Xu A, Zhang Y. et al. / Current Applied Physics, 2010, v.10, p.967–970

8. Kandalkar S.G., Gunjakar J.L., Lokhande C.D. et al. / Journal of Alloys and Compounds, 2009, v.478, p.594–598

9. Toniolo J.C., Takimi A.S., Bergmann C.P. / Materials Research Bulletin, 2010, v.45, p.672–676

10. Ed L., Gabriele A., Jun L. et al / Progress in Crystal Growth and Characterization of Materials, 2012, v.58, p.3–13

11. Kishore P. N. R. andJeevanandam P. / Journal of Nanoscience and Nanotechnology, 2013, v.13, p.2908-2916

12. Azadeh A., Ali M. / UltrasonicsSonochemistry, 2009, v.16, p.124–131

13. Xuemin H., Xueyin S., Wen Q. et al. / J. Phys. Chem. C, 2015, v.119, p.9550–9559

14. Kundu S., Jayachandran M. / J Nanopart Res., 2013, 15:1543

15. Barakat A.M., Khil M.S., Sheikh F.A. et al. / J. Phys. Chem. C, 2008, v.112, p.12225–12233

16. Chattopadhyay S., Chakraborty S.P., Laha D. / Cancer Nano, 2012, 3:13–23

17. Chen M., Xia X., Zhang J. et al. / Materials Research Bulletin, 2016, v.74, p.472–477

18. Raghavender T., Ramesh K. G., Pravansu S. M. et al. / Journal of Power Sources, 2012, v.209, p.44–51

19. Xu M., Wang F., Zhao M. et al. / ElectrochimicaActa, 2011, v.56, p.4876–4881

20. Vetter S., Haffer S., Wagner T. et al. / Sensors and Actuators B: Chemical, 2015, v.206, p.133-138

21. Ronan B., Gregory C., Sabine V. / UltrasonicsSonochemistry, 2017, v.36, p.27–35

22. Haldorai Y., Kim J.Y., EzhilVilian A.T. et al. / Sensors and Actuators B: Chemical, 2016, v.227, p.92-99

23. Moon J., Kim T.K., VanSaders B. et al. / Solar EnergyMaterials&SolarCells, 2015, v.134, p.417–424

24. Wang L., Song X., Zheng Y. / Micro & Nano Letters, IET, 2012, v.7, p.1026-1029

25. Sathish S., Chandar S. B., Manivannan N. / Iran Polym J, 2015, 24:63–74

26. Yahya H.F., Ghada A. M. et al. / Journal of Radiation Research and Applied Sciences, 2014, v.7, p.135-145

27. Ozkaya T., Baykal A., ToprakM.S.and et al. / Journal of Magnetism and Magnetic Materials, 2009, v.321, p.2145–2149

28. Muradov M.B.,Balayeva O.O., Azizov A.A. et al / Infrared Physics&Technology, 2018, v.89, p.255-262.

THE EMERGENCE OF DRIFT CAPACITY IN 2D InSe CRYSTALS

A.G. GUSEINOV[1], V.M. SALMANOV[1*], R.M. MAMEDOV[1], A.A. SALMANOVA[2], F.SH. AHMADOVA[1], N.D. DASHDAMIROVA[1]

[1]Baku State University, AZ 1148 Baku, Azerbaijan,
[2]Azerbaijan State University of Oil and Industry, Baku, Azerbaijan

I – V characteristics and current kinetics under the action of a laser pulse in ultrathin InSe films, 1.3 μm thick, delaminated from a single-crystal ingot by mechanical means were studied. The saturation of the current in I – V characteristic at high fields is explained by the limitation of the injection of electrons from the source. When a film is excited by a laser pulse with duration of 12 ns, a drift capacitance arises in it, which discharges after the termination of the laser pulse and the current relaxation can be viewed as a dissipative relaxation-type flow and apply Maxwell – Cattaneo equations to it.

1. INTRODUCTION

Among 2D materials, the most promising for nanoelectronics and photonics is the atomically thin film of indium selenide [1-4]. The advantages of a 2D InSe crystal over other 2D materials, such as graphene, silicon, Mo_2S, etc. this is due to the fact that InSe has a very high mobility of conduction electrons [5, 6] with a relatively short lifetime of non-equilibrium current carriers and high mechanical flexibility of ultrathin films [7–9]. When the number of monolayers decreases from twenty to two layers, the band gap of ultrathin films of indium selenide varies in the range from 1.26 eV to 1.66 eV [8, 10]. Consequently, ultrathin layers of indium selenide can be in demand for the manufacture of high-speed and high-performance photodetectors operating in the near infrared region of the spectrum. However, ultrathin InSe films consisting of several monolayers, i.e. several hundred angstroms thick, have a low absorption coefficient value [11], which somewhat overshadows the material prospects for photoelectronics.

This paper presents the results of studies of the electrical and photoelectric properties of 1.3 mm thick InSe thin films, which is comparable with the wavelength of the corresponding fundamental absorption edge of a crystal with a high absorption coefficient.

2. EXPERIMENTAL

Tonkin InSe films are obtained by mechanically peeling a film from a single-crystal ingot. Monocrystalline ingots of indium selenide were obtained by the Bridgman method in the horizontal version. Samples $(4 \times 4 \times 10)$ mm^3 were cut from the middle section of the ingot, and then several layers were peeled off from the surface (4×4) mm^2 perpendicular to the c axis of the crystal. From the last layer located on the adhesive tape, more layers were removed to obtain an ultrathin film with a thickness of 1.3 μm. Figure 1 shows the SEM image of the film edge, which allows determining the film thickness.
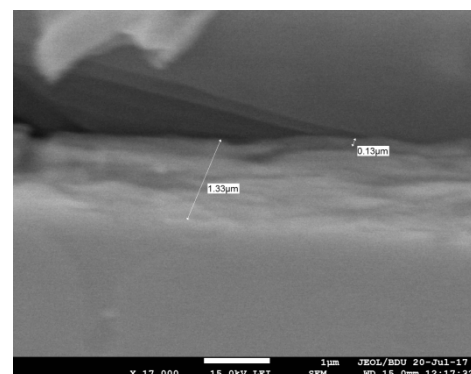

Figure 1.Image on SEM edge of thin film InSe.

The thickness of each monolayer in InSe is 63 Å, therefore, the film consists of 100 monolayers. Conductive contacts of low-resistance silver paste were

9

deposited on the resulting film.

The volt-ampere characteristic of the samples was taken in the mode of constant and alternating currents without connecting the load resistance using the TR-4805 characterograph. To study the photoelectric properties of the samples, a halogen lamp with a quartz base, a monochromator of type M833 with double dispersion, a pulsed Nd +: YAG laser with generation of the second and third harmonics were used. The duration of the laser radiation was 12 ns, with a maximum power of 7 MW/cm^2.

3. RESULTS AND DISCUSSION

Mechanisms of current passage in 2D-crystals may differ significantly from bulk crystals. In atomically thin films, the number of lattice defects, including the amount of foreign impurities, is reduced to zero, and the material has almost intrinsic conductivity. Therefore, currents that depend on temperature and on external influences (for example, light) in two-dimensional crystals are limited by the number of free charge carriers injected from the source, similar to currents limited by the volume charge in high-resistance crystals. However, unlike three-dimensional, in two-dimensional crystals along with ionized atoms, neutral lattice atoms occupying a certain portion of the cross section of atomically thin films can play the role of a shielding element and cause resistance for charge carriers, reducing their mobility. I – V characteristic of an ultrathin InSe film 1.3 μm thick shown in Figure 2 clearly demonstrates the above-mentioned assumption. The length of the film between the conductive contacts (between the source and drain) was 4 mm, therefore in the range of the field strength 0-400 V/cm, the characteristic obeys Ohm's law and the current density in the sample is determined by the expression:

$$j = e(n\mu_n + p\mu_p)E . \tag{1}$$

Considering that the film has n-type conductivity and the electron mobility in ultra-thin InSe films (μ$_n$ = 720 cm^2/V·s) far exceeds the hole mobility, equation (1) can be written as:

$$j = en\mu_n E . \tag{2}$$

Starting at 400 V/cm, the current is saturated in the sample, which is caused by the restriction of

electron injection due to the small cross section of the film. Taking into account the cross section of the film (4·10^{-9} m^2), using the formula (2), we calculate the maximum concentration of electrons injected from the source: $n \approx 7 \cdot 10^{13}$ sm^{-3}.

In the field of strong fields (E> 400 V/cm), the current through the sample increases slightly. In all likelihood, this is due to the field dependence of the electron mobility. When the film is illuminated with white light with an intensity of 160 and 200 Lux, non-equilibrium charge carriers are generated in the film, and the current increases accordingly. From curves 2 and 3 in Figure 2, it can be seen that the sublinearity of the characteristics of the illuminated sample begins at lower field strengths. However, the resistance of the samples at small fields and different levels of illumination are equal. This means that the concentration of generated non-equilibrium charge carriers also saturates, and the increase in current in the region of high fields and levels of optical excitation is necessarily caused by an increase in the mobility of charge carriers. High electron mobility and ultrathin structure, i.e. The 2D format of the film contributes to the appearance of drift capacitance when current passes through the film.
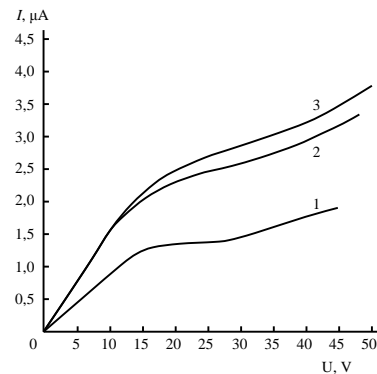
Figure 2. I – V characteristics of a thin film InSe, 1.3 microns thick. 1- in the dark; 2 - when illuminated 160 lux, 3 - when illuminated 200 lux.

Since highly mobile electrons leave the sample sink, and slow-moving holes slow down the injection of electrons from the source, a negative charge accumulates around the source (Fig. 3). Thus, a positive charge accumulates at the drain (anode) of the sample, and a negative charge at the source (cathode). With a steady flow of current, the drift capacitance has a small value. However, when a film is illuminated by

10

a laser pulse, a photocurrent pulse arises due to nonequilibrium electrons and holes. Extraction of high-mobility electrons near the anode and recombination of slow-moving holes contributes to the appearance of a large drift capacitance.
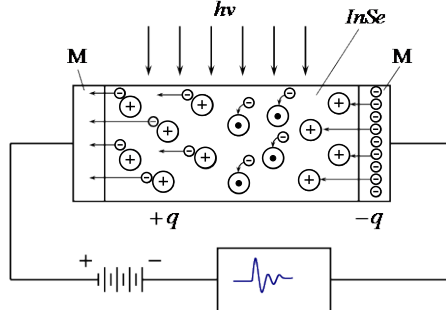
Figure 3. Diagram illustrating the occurrence of drift capacity in InSe.

An 1.3 µm-thick InSe film was irradiated with a laser pulse of 12 ns duration and a wavelength of 535 nm. As a result, an equal number of nonequilibrium electrons and holes was generated. Electrons with high mobility quickly leave the film runoff. After the cessation of illumination, in the middle of the film, a part of nonequilibrium holes recombines with electrons and a high-resistance region of neutral atoms is formed.

Thus, after the cessation of optical excitation, along with the usual relaxation of the photocurrent caused by the recombination of nonequilibrium charge carriers, the drift capacitance formed by the region of charged positive ions in the near-anode region of the film and the cathode electrons also discharge. Therefore, the relaxation process can be considered as a dissipative flow of the relaxation type and apply the Maxwell-Cattaneo equations to it [12]:

$$j + \tau \frac{dj}{dt} = -\sigma \nabla \varphi , \qquad (3)$$

where j –current density, τ – photocurrent relaxation time, σ – film electrical conductivity, $\varphi = \dfrac{q}{C}$ – potential transfer capacity due to drift.

At zero gradient of the transfer potential, i.e. the absence of the process of the drift capacitance in the film, single-channel recombination of non-equilibrium charge carriers occurs according to the law:

$$j = -\tau \frac{dj_f}{dt} . \qquad (4)$$

where j_f –current density. The photocurrent density with constant electron mobility can be expressed by the formula:

$$j_f = e\Delta n\upsilon = \frac{eN}{V}\upsilon = \frac{q}{V}\upsilon , \qquad (5)$$

where, V – film volume, υ – electron drift velocity, $q = eN$ – the number of non-equilibrium electrons decreasing over time by the formula:

$$q(t) = q_0 e^{-\frac{t}{\tau}} , \qquad (6)$$

where, q_0 – the amount of non-equilibrium electrons generated by laser radiation.

The discharge of positive and negative charges of the drift capacitance through the measuring circuit, will occur according to the law:

$$q' = q'_0 e^{-\delta t} \cos \omega t , \qquad (7)$$

Where q'_0 – charge drift capacitance at the time of termination of optical excitation, δ – logarithmic damping decrement, ω – natural frequency of the measuring circuit. The transfer potential due to the field between the cathode and anad is equal to:

$$\varphi = \frac{q'}{C} = \frac{q'_0}{C} e^{-\delta t} , \qquad (8)$$

Where C – drift capacity. Potential gradient $\nabla \varphi$ determined only in the direction of current flow over a distance ℓ, between the anode and cathode, and it can be written with a simple expression φ/ℓ.

Taking into account equations (5), (6) and (7) in (3), we obtain the expression for the relaxation of the photocurrent pulse in thin films of the type InSe:

$$i = j \cdot S = \frac{\upsilon q_0}{\ell} e^{-\frac{t}{\tau}} - \frac{q'_0 \sigma S}{C\ell} e^{-\delta t} \cos \omega t , \qquad (9)$$

where S – cross section of thin film. The pre-exponential factors are constant, independent of time for a given thin film. Therefore, equation (9) can be written as:

$$i = Ae^{-\frac{t}{\tau}} - A'e^{-\delta t} \cos \omega t , \qquad (10)$$

where, $A = \dfrac{\upsilon q_0}{\ell}$, $A' = \dfrac{q'_o \sigma S}{C\ell}$ .When choosing values for constant A = 0.08; A′ = 0.05; τ = 0.5 ns; $\delta = 0,05$ ns⁻¹ and ω = 20 ns⁻¹, dependence $i(t)$ calculated by formula (10) has the form shown in Fig. 4. The photocurrent kinetics in ultrathin InSe films under the action of pulsed laser radiation with duration of 12 ns is shown in Fig. 5. Comparing the calculated and experimental dependences of the relaxation current on time, we observe good consistency between them. Thus, equation (9) can be used for mathematical modeling of current pulse relaxation in ultrathin 2D crystals of the indium selenide type. In this case, it is meant that the properties of indium selenide should be taken into account. As noted above, the electron mobility in InSe nanolayers is many times greater than the hole mobility. This feature is necessary for the appearance of drift capacitance in 2D crystals.
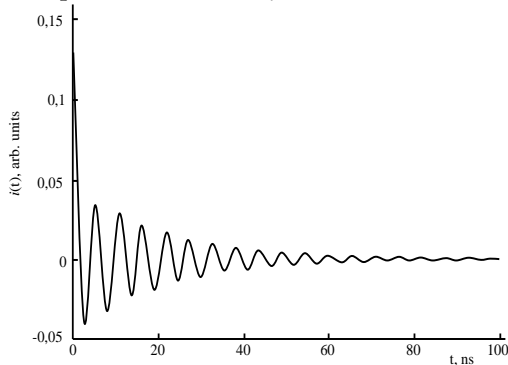
Figure 4.Calculated current versus time using Maxwell-Cattaneo equation.
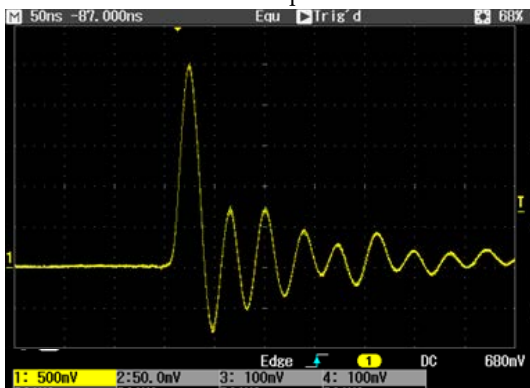
Figure 5.Experimental time dependence of the relaxation current in ultrathin InSe films under the action of pulsed laser radiation.

The main parameters of standart and nano-granular solar cells on the basis of $TiO_2/Cd_{0.1}Zn_{0.9}S_{0.2}Se_{0.8}/Si$ heterojunctions are shown in Figure 2.

4. CONCLUSION

The saturation of the current in ultrathin InSe films is due to the restriction of the injection of electrons from the cathode. When the film is illuminated with white light, the concentration of generated nonequilibrium charge carriers also saturates, and the increase in current in the region of high fields and levels of optical excitation is necessarily due to an increase in the mobility of charge carriers. After optical excitation of the film by a light pulse with a duration of tens of nanoseconds, along with the usual relaxation of the photocurrent caused by the recombination of nonequilibrium charge carriers, the drift capacitance formed by the region of charged positive ions in the near-anode region of the film and the cathode electrons also occurs. Therefore, the relaxation process can be considered as a dissipative flow of the relaxation type and the Maxwell-Cattaneo equations can be applied to it.

5. RREFERENCES

1. Mudd G.W., Patane A.,Kudrynskyi Z. R., Fay,M. Makarovsky W.O., Eaves L., Kovalyuk Z.D., ZólyomiV., and FalkoV.. Appl. Phys. Lett. 105, (2014), 221909, https://doi.org/10.1063/1.4903738
2. Nilanthy Balakrishnan, Zakhar R Kudrynskyi, Emily F Smith, Michael W Fay, Oleg Makarovsky, Zakhar D Kovalyuk, Laurence Eaves, Peter H Beton, Amalia Patane. 2D Materials. 4, (2017), 025043/1.
3. Liu Q., LiX., Xiao Z. Y. Zhou, H. Chen, Khali A. l, T. Xiang, J. Xu, W. Chu, X. Wu, J. Yang, C. Wang, Xiong Y., Jin C., Ajayan P.M., Song L., Advanced Materials. 27(33), (2015), 4837.
4. Srinivasa Reddy Tamalampudi, Yi-Ying Lu, Rajesh Kumar U., Raman Sankar, Chun-Da Liao,

12

Karukanara Moorthy B., Che-Hsuan Cheng, Fang Cheng Chou§, Yit-Tsong Chen. Nano Lett. 14(5), (2014), 2800.

5. Po-Hsun Ho, Yih-Ren Chang, Yu-Cheng Chu, Min-Ken Li, Che-An Tsai, Wei-Hua Wang, Ching-Hwa Ho, Chun-Wei Chen, and Po-Wen Chiu. ACS Nano. 11(7), (2017), 7362.

6. Danil W. Boukhvalov, Bekir Gürbulak, Songül Duman, Lin Wang, Antonio Politano, Lorenzo S. Caputi, Gennaro Chiarello, Anna Cupolillo. Nanomaterials. 7, (2017), 372; doi:10.3390/nano7110372.

7. Bandurin D.A., Tyurnina A.V., Yu G.L., Mishchenko A., Zolyomi V., Morozov S.V., Kumar R.K., Gorbachev R.V., Kudrynskyi Z.R., PezziniS., Kovalyuk Z.D., Zeitler U., Novoselov K.S., Patane A., Eaves L., Grigorieva I. V., V. Fal'ko I., Geim A. K., and Cao Y. Nature Nanotechnology. 2017, 12(3), 223.

8. Chaoyu Song, Fengren Fan, Ningning Xuan, Shenyang Huang, Guowei Zhang, Chong Wang, Zhengzong Sun, Hua Wu, Hugen Yan. L ACS Appl. Mater. Interfaces. 10 (4), (2018), 3994.

9. Tao Wang, Jianwei Li, Hao Jin, Yadong Wei. Phys. Chem. Chem. Phys. 20, (2018), 7532.

10. Mauro Brotons-Gisbert, Daniel Andres-Penares, Joonki Suh, Francisco Jesus Hidalgo, Rafael Abargues, Pedro J. Rodriguez-Canto, Alfredo Nava Segura, Ana Cros, Gerard Tobias, Enric Canadell, Pablo Ordejón, Junqiao Wu, Juan P Martinez-Pastor, J. F. Sánchez-Royo. Nano Letters, American Chemical Society (ACS). 2016, 16(5), DOI: 10.1021/acs.nanolett.6b00689.

11. J. Hossain, M. Julkarnain, K. S. Sharif, K. A. Khan. Journal of Scientific Research & Reports. 2014, 3(12), 1642.

12. Martin Ostoja-Starzewski. International Journal of Engineering Science, 2009, 47, Issues 7–8, 807.

13

SYNTHESIS AND STABILIZATION OF BIMETALLIC Fe/Ni AND Fe/Cu NANOPARTICLES

G.G.VALIYEVA[1*], LUCA DI PALMA[2], S.R.HAJIYEVA[1], M.A.RAMAZANOV[3], F.V.HAJIYEVA[3]

[1]Baku State University, Department Ecological Chemistry, Ecology and Soil science faculty, AZ1148, Baku, Azerbaijan
[2]SapienzaUniversita` di Roma, Dipartimento di Ingegneria Chimica Materiali Ambiente, Via Eudossiana 18, 00184 Rome, Italy
[3] Baku State University, Department Chemical Physics of Nanomaterials, Faculty of Physics, AZ1148, Baku, Azerbaijan

In this paper bimetallic nanoparticles on the base Fe/Ni and Fe/Cu were synthesized in the presence of different surface-active substance medium by borohydride reduction method under nitrogen conditions. The characterization of the bimetallic nanoparticles was performed using XRD, SEM and AFMtechniques. It was found that in the presence of sodium oleatesurfactant, bimetallic nanoparticles were more effective stabilized against oxidation and agglomeration. It was also determined that in the presence of sodiumoleatestabilizer produced stable, well-dispersed bimetallic nanoparticle solutions. Electron microscopic studies have shown that the particle size for monometallic iron nanoparticles is 40-80 nm, for bimetallic nanoparticles Fe/Ni and Fe/Cu- 10-60 nm.

1. INRODUCTION

In the last decade, zero-valent iron as a reductant and efficient agent has been used in water and soil treatment to decrease the concentration of environmental pollutants under toxicity limit. NZVI nanoparticles possess unique physical and chemical properties different from bulk material. They have many potential applications in environment.

Coating of nanoiron with other metals such as Cu, Ni, Pd, Pt and Ag has been proposed for treating a number of contaminants in water and soil. Bimetallic nanoparticles have a higher reaction rate compared to those observed for nZVI alone [3]. Recently, bimetallic nanoparticles have received considerable attention because of their importance for magnetic, optical, and catalytic applications in a variety of fields; their value arises from their distinctive properties, which are clearly different from those of monometallic nanoparticles.

Generally, bimetallic nanoparticles can be categorized into two main groups: core–shell and alloys structures. Depending on the synthetic approach used in the preparation of bimetallic nanoparticles, the spreading of every metal in a particleand their organization will vary to adopt either core–shell, random alloy, alloy with an intermetallic compound type or cluster-in-cluster, subclusters, etc. The mechanism responsible for their reactivity is related to catalytic hydrogenation and electrochemical effects [4]. It was indicated that coating of nZVI by second metal decreases the aggregation and agglomeration of nZVI, in addition to enhancing the rate of reduction in aqueous solution for treatment pollutants [5]. However, the efficiency of the catalyst used in bimetallic nanoparticles decreases during time due to formation of an iron hydroxide layer, which hinders the contact between the reactants and the catalyst [6].

In the bimetallic nanoparticles with cluster-in-cluster structures, onenanoclustersact with other nanoclusters as a binder. The cluster-in-cluster structure may be considered as a modification of the core–shell structure. It has been reported that heterogeneous bimetallic nanoparticles have more properties than the single component metal nanoparticles, according to their tunable chemical and physical properties [2]. The properties of bimetallic nanoparticles can be tuned by adjusting composition, atomic ordering, morphology, and size. Bimetallic nanoparticles are the multifunctional nanomaterials

14

with applications in different fields: environment, industry, technology. Researchers are trying to synthesize more and more new bimetallic nanoparticles with desired and controlled geometrical as well as magnetic properties. It can also be concluded that bimetallic nanoparticles are of greater importance as compared to monometallic nanoparticles because of enhanced properties. These particles have greater surface area, as a result of which they act as catalyst and helps in effectively catalyzing various reactions.

In this review reported the stabilization of bimetallic particles in aqueous media in the presence of surfactants as stabilizers. It is desirable to have the flexibility of using nanoparticles both in the liquid and solid phases, preferably with the same matrix and stabilizer. Additionally, using iron as the main catalysts gives to us opportunity to easily recover after the reaction and hence avoid elaborating separation procedures, due to its magnetic properties.

In the present study, stabilized bimetallic nanoparticles containing Fe by Ni and Cu were synthesized in the presence of surface-active substance-sodium oleate and characterized by different techniques (XRD, SEM, EDS). Experiments were carried out in batch mode under strong agitation in the presence and absence of dissolved oxygen.

2. EXPERIMENTS AND METHODS

2.1. Materials

Iron (III) chloride hexahydrate (PLC 141358 - 99 % chemically pure), sodium borohydride (PLC 143314 - 99 % chemically pure), nickel (II) sulphate heptahydrate (PLC 141445, 98 % chemically pure), copper sulphat epentahydrate (PLC 175639), sodium oleate
($C_{18}H_{33}NaO_2$PLC - 113655) and ammonia solution (28- 30%) were used for nZVI and bimetallic Fe/Ni and Fe/Cu particles synthesis. All chemicals were of analytical grade and were used as received without further purification.

2.2. Synthesis and stabilization of Fe/Ni and Fe/Cu bimetallic nanoparticles

Bimetallic nanoparticles were synthesis in a flask reactor with three open necks. To avoid the agglomerating, dispersing agents were used during synthesis. Several dispersing agents were evaluated in this work including sodium oleate (SO), carboxymethylcellulose sodium salt (CMC), cetyltrimethylammonium bromide (CTABr), polyethylene glycol (PEG). It was found that in the presence of sodium oleatesurfactant, bimetallic nanoparticles were more effective stabilized against oxidation and agglomeration. Of these, SO was found to disperse nanoparticles well, than others which stabilize not well and oxidise faster.

Bimetallic nanoparticles were prepared by mixing 0.1M Fe^{3+}solution with30 ml of 0.5% solution of sodium oleate. It was well mixed on a magnetic stirrer at 500 rpm. After 15 min, different amount of the second metal(Ni and Cu) was added into the solution for test which loading of the second metal is better (0.1%, 0.3% and 0.5%). On the other hand, 100 ml0.3 M sodium borohydridesolution was prepared and added into the above solution dropwise and stirred constantly. All the reaction was at room temperature and in a free oxygen atmosphereunder nitrogen gas. The mixture was left for another 10 minutes of stirring after adding sodium borohydride solution, so that the reaction was complete.

For complete removal of non-reactive ions synthesized bimetallic nanoparticles were washed 3 times with absolute ethanol. CR4000 pro-Analytical centrifuge was used for nanoparticles washing.

3. RESULTS AND DISCUSSION

3.1. Characterization of the so-bnp system

SEM Analysis. The morphologies of bimetallic Fe/Ni and Fe/Cu nanoparticles have been studied by scanning electron microscopy (SEM, JEOL JSM-7600 F). Scanning was carried out in SEI mode with an accelerating voltage of 15 kV and a working distance of 4.5 mm. Figure 1 shows the SEM image of freshly synthesized nZVI nanoparticles without additional of the second metal and bimetallic nanoparticles on the base Fe/Ni and Fe/Cu. It can be observed that the iron particles are in the form of nanospheres, which exist in contact with each other and form chains having diameters of 40-80 nm. Butbimetallic nanoparticles (Fe/Ni and Fe/Cu) shows significantly difference in size distribution. As seen in SEM analysis, size of bimetallic nanoparticles became dramatically less after addition of the second metal, approximately 10-60

nm.The particles were well dispersed and the specific surface area of particles increased due to the joining of the second metal. Figure 2 and 3 shows the energy-dispersive spectrum and mapping of nZVI and bimetallic nanoparticles (Fe/Ni and Fe/Cu). As can be seen from Figure 2 and 3 the synthesized nanoparticles belong to bimetallic Fe/Ni and Fe/Cu nanoparticles.
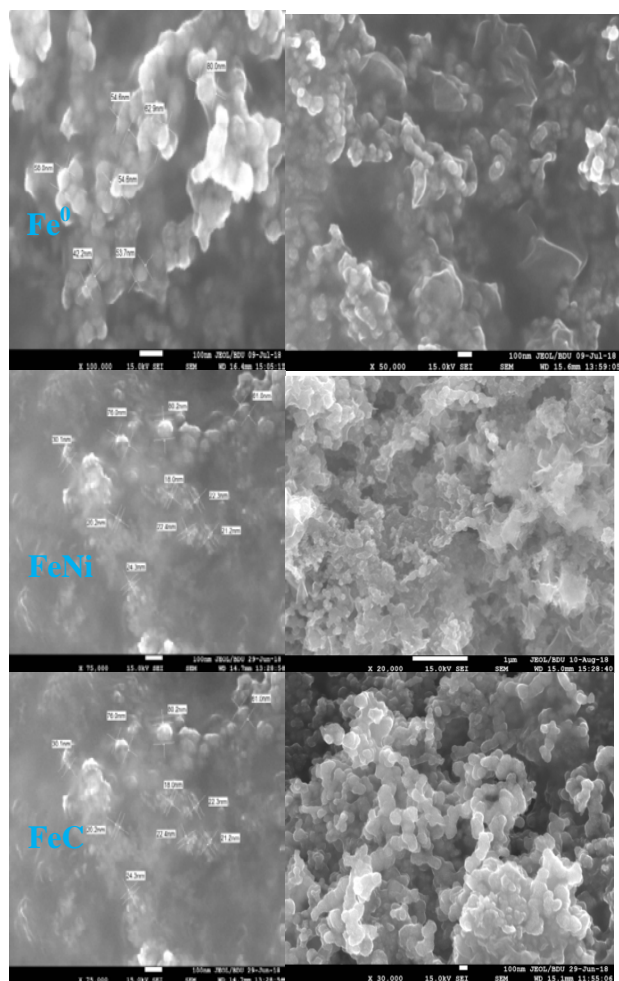
Figure 1. SEM images of nZVI particles and 0.5% the second metal loading bimetallic (Cu,Ni) nanoparticles.

*XRDanalysis.*X-ray diffraction analysis of bimetallic nanoparticles was performed on Rigaku Mini Flex 600 XRD diffractometer at ambient temperature. In all the cases was used Cu Kα radiation from a Cu X-ray tube (run at 15 mA and 30 kV) and scan area was 20~80°. When the standard deviation is higher (~4.82), the phase may not be detectable by XRD. This limitation of XRD has amorphous structure, which exhibits only short-range ordering. XRD of FeNi and FeCu bimetallic nanoparticles determined amorphous phase.
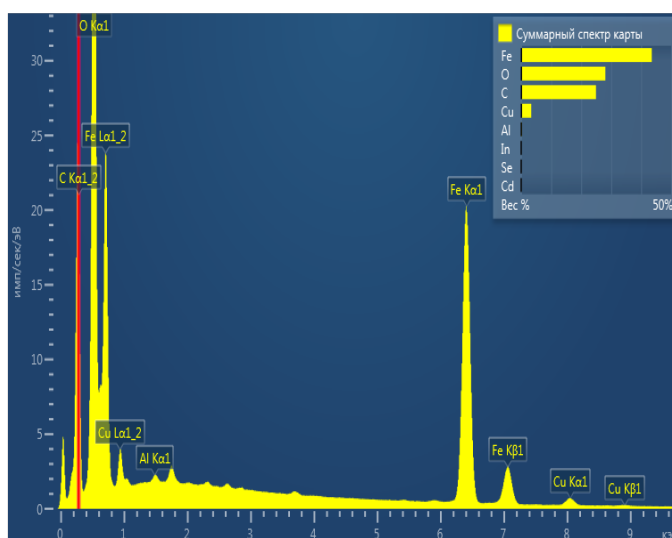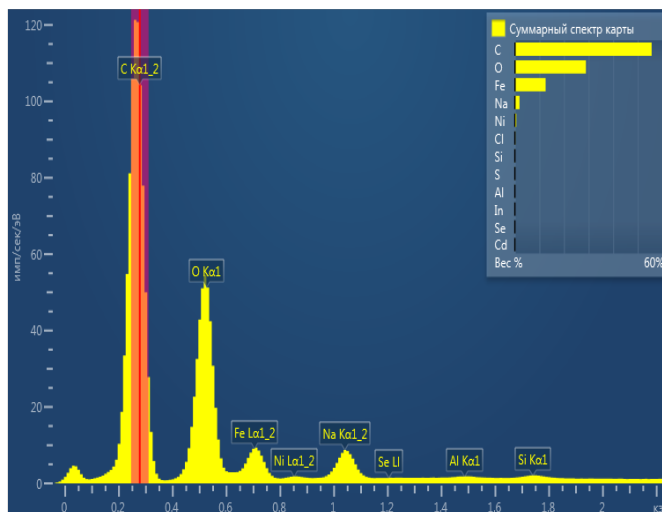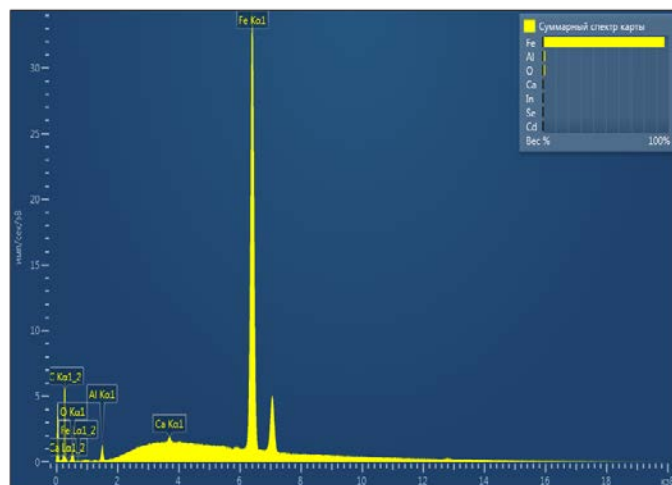
Figure 2.EDS spectra of nZVI particles and the Fe/Cu and Fe/Ni bimetallic nanoparticles

16
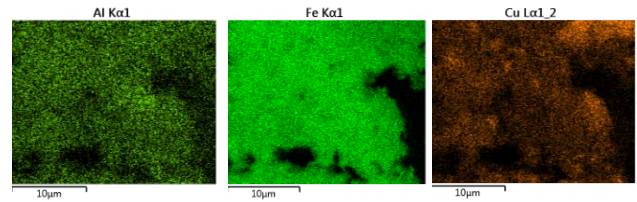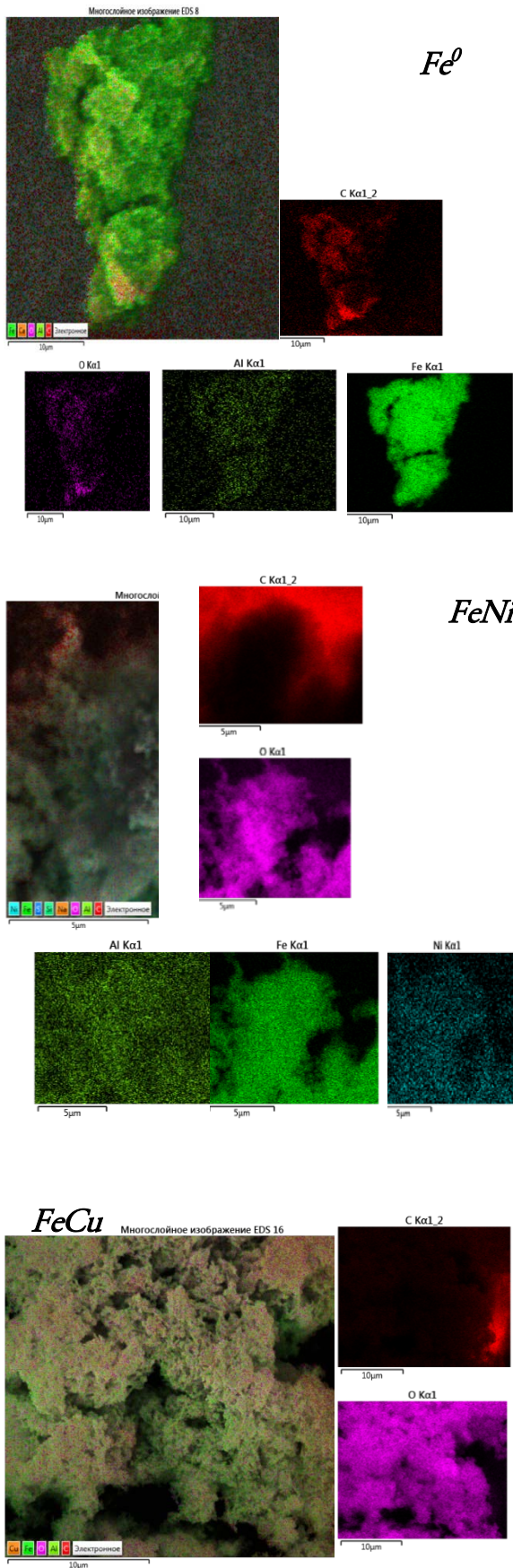
Figure 3. Mapping of nZVI particles and the Fe/Cu and Fe/Ni bimetallic nanoparticles

AFM analysis. The morphology of nanoparticles was studied by using Integra-Prima (NT-MDT, Zelenograd). A special silicon cantilever, prepared by plasma chemical method of etching with radius of curvature of needle 20 nm and resonance frequency 1–5 Hz was used. The measurement was implemented in semi contact mode in air, where the vibration of cantilever needle, that determines the surface topography was fixed. The scanning rate and scanning lines number on the image are 1.969 Hz and 256 Hz, respectively. AFM results show that the average size of iron nanoparticles is 30-90 nm and for Fe/Ni-26-45 nm. As can be seen, SEM and AFM studies correlate well with each other.
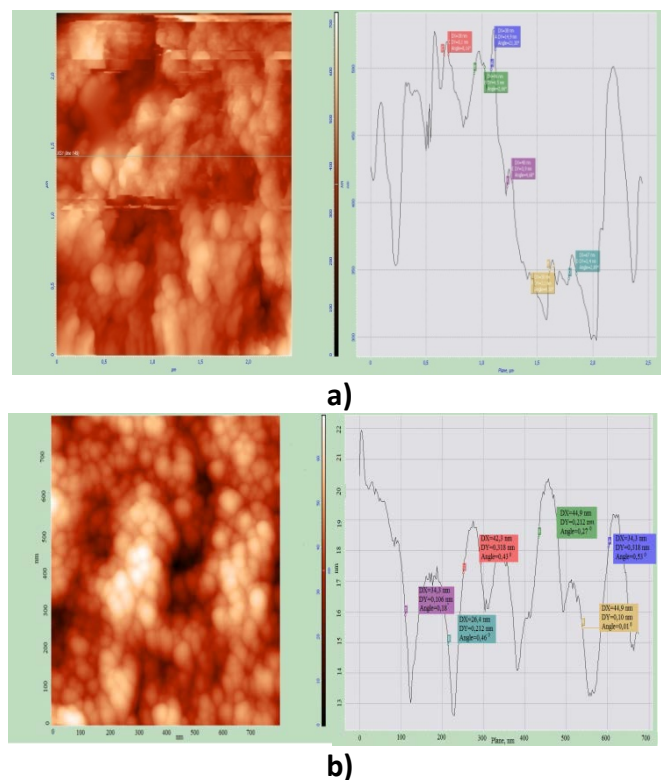
Figure 4. AFM 2D of the surface and size distribution of the Fe (a) and Fe/Ni (b) nanoparticles.

17

4. CONCLUSIONS

Bimetallic nanoparticles on the base Fe/Ni and Fe/Cu were synthesized in the presence of different surface-active substance medium by borohydride reduction method under nitrogen conditions. The characterization of the bimetallic nanoparticles was performed using XRD, SEM and AFM techniques. It was found that in the presence of sodium oleatesurfactant, bimetallic nanoparticles were more effective stabilized against oxidation and agglomeration. It was also determined that in the presence of sodiumoleatestabilizer produced stable, well-dispersed bimetallic nanoparticle solutions. Electron microscopic and AFM studies have shown that the particle size for monometallic iron nanoparticles is 40-80 nm, for bimetallic nanoparticles Fe/Ni and Fe/Cu- 10-60 nm.

5. REFERENCES

1. Nasrabadi, H.T., Abbasi, E., Davaran, S., Kouhi, M., & Akbarzadeh, A. (2014). Bimetallic nanoparticles: Preparation, properties, and biomedical applications. Artificial Cells, Nanomedicine and Biotechnology, 44(1), 376–380.
2. Sharma, G., Gupta, V.K.,Agarwal, S., Kumar, A., Thakur, S., Pathania, D. Fabrication and characterization of Fe@MoPO Nanoparticles: Ion exchange behavior and photocatalytic activity against malachite green. J. Mol. Liq. 2016, 219, 1137–1143.
3. Tratnyek P.G., Schere M.M., Johnson T.J., Matheson L.J., Permeable reactive barriers of iron and other zero-valentmetals, In: M.A. Tarr (Ed.), Chemical Degradation Methods for Wastes and Pollutants: Environmental and Industrial Applications, Marcel Dekker, New York, NY, pp. 371–421, 2003.
4. Mossa Hosseini S., Ataie-Ashtiani B., Kholghi M., Nitratereduction by nano-Fe/Cu particles in packed column, Desalination 276 (2011) 214–226.
5. Tie Li., J. Farrell, Reductive dechlorination of trichloroetheneand carbon tetrachloride using iron and palladized-ironcathodes, Environ. Sci. Technol. 34 (2000) 173–179
6. Liou Y.H., Lo S.L., Lin Ch.J., Kuan W.H., Weng Sh.Ch.,Chemical reduction of an unbuffered nitrate solution using catalyzed and uncatalyzednanoscale iron particles, J. Hazard. Mater. 2005,127, 102–110.
7. Santos F.S., Lago, F.R., Yokoyama, L., & Fonseca F.V. (2017). Synthesis and characterization of zero-valent iron nanoparticles supported on SBA-15. Journal of Materials Research and Technology, 6(2), 178–183.
8. Yuvakkumar R., Elango V., Rajendran V., Kannan N., Digest Journal of Nanomaterials and Biostructures, Vol. 6, No 4, October-December 2011, p. 1771-1776.

INFLUENCE OF CONCENTRATION OF Ag+ IONS IN SOLUTIONS TO PHYSICAL PROPERTIES OF CdS NANOPARTICLES

L.R.GAHRAMANLI[1*], M.B. MURADOV[1], Á. KUKOVECZ[2], O.O. BALAYEVA[3], G.M. EYVAZOVA[1], S.Z. HUSEYNLI[1], H.A. SHIRINOVA[1]

[1]Department of Physics, Baku State University, Z. Khalilov str., 23, AZ-1148 Baku, Azerbaijan
[2]Department of Applied and Environmental Chemistry,University of Szeged ,Szeged, Hungary
[3]Department of Chemistry, Baku State University,Z.Khalilov str.,23,AZ-1148 Baku, Azerbaijan

In the present work, we were study the influence of ion exchange process of CdS nanoparticles with silver ions to optical and structural properties. CdS nanoparticles were synthesized by sonochemical method. After obtaining powder of CdSnanoparticles, ion exchange process was carried out in different concentrate. The effects of the ion exchange process on the optical and photoluminescence properties of CdS nanoparticles have been studied by X-ray Diffraction (XRD),UV-Visible, Infrared spectroscopes and spectrofluorimeter (PL).

1. INTRODUCTION

The interest in studying particles at the nanometer – size is related to changing of optical and electrical properties depending on the particle size. In nanoparticles preparation, it is very important to control the particle size, particle shape and morphology [1].Semiconductor nanoparticles attract considerable attention due to width of application areas. The interest in element of II-VI groups is related to their potential technological application. Nanometer sized particles display many interesting optical, electronic, magnetic and chemical properties yielding applications in biological nano sensors, optoelectronics, nano devices, nano electronics, information storage and catalysis[2].

Recently, there has been growing interest in the study of nanomaterials due to their unique physical and chemical properties and potential applications in the fields of catalysis [3],photocatalysis [4],solar cells [5] and sensors [6] etc.CdS is one of the interesting materials of II-VI group's semiconductors. The prominent application fields of CdS is nonlinear optical devices, flat panel displays, light emitting diodes, lasers, logic gates, transistors, etc [7-9]. In the synthesis of nanoparticles by chemical methods, using of capping agents, allows that control of the particles size and to prevent agglomeration of the synthesized particles.

The optical properties of semiconductor CdS nanoparticles can vary over a wide visible range depending on the particle size due to the quantum-confined effect [10]. The morphology, degree of crystalline, surface state of nanoparticles, their interaction with the substrate and with each other also affects their optical properties [11-15]. It is possible to obtain strong affinity to ions, high absorption capacity and well-dispersed nanoparticles by ion exchange process. Currently, the sonochemical method has been used extensively to generate novel materials with unusual properties, since they form particles of a much smaller size and higher surface area than those reported by other methods [16].

In this study, we were synthesized CdS nanoparticles with sonochemical method. After that, the effect of ion exchange on the optical properties of synthesized nanoparticles was investigated.

2. EXPERIMENTAL

2.1. Synthesis of CdS nanoparticles

0.01M solution of Cd $(CH_3COO)_2 \cdot 2H_2O$ and 0.07 M solution of Na_2S were separately dissolved in 50 ml distilled water. 5% of 3-Mercaptopropionic acid was used as capping agent. For exposing oxygen gas from the reaction medium. The reaction medium was continuously affected with nitrogen gas. Reaction was carried out for 2 hours. The yellow precipitate-

19

CdSnanoparticles were formed. The final solution were centrifuged, washed with distilled water and then alcohol and dried at room temperature.

2.2. Ion exchange of CdS nanoparticles with Ag⁺ ions

For ion exchange of CdS nanoparticles with Ag⁺, two different concentration- 0.005M and 0.1M of $Ag(NO_3)_2$ were added in CdS dried powder, separately. In small concentration - 0.005M of solution of ion exchange of CdS nanoparticles with Ag⁺ ions (*sample 1*) gradually turns into black color.In 0.1M of solution of ion exchange of CdS nanoparticles with Ag⁺ions(*sample 2*) suddenly turns into a black color. Changing of optical properties has been studied with UV-visible.

3. RESULT AND DISCUSSION

3.1. X-ray diffraction

The X ray diffraction (XRD)patterns for cadmium sulfide and ion exchanging samples of cadmium sulfide were recorded on a Rigaku Miniflex 250 with Cu Kα radiation (Cu Kα: λ = 1.5406 Å) with 2θ ranging from 20° to 60°. The XRD is the ideal technique for determining the structural structure of the samples, the crystallite size and identify of samples compared to the literature.The XRD patterns of the prepared samples of cadmium sulfidenanoparticles and ion exchanging samples of cadmium sulfide are shown in Figure 1.

The XRD patterns of the CdS samples and Sample 1 exhibit a single phase cubic structure. The peaks with 2θ values of 25.87°, 43.10°, 53.07° for CdS nanoparticles, respectively,26°,43°,55° for Sample 1 correspond to the (110), (220), (311) planes of the cubic phase CdS (JCPDS Card No. 10-0454). Figure 1.c show the XRD pattern of the sample 2, containing silver sulfide nanoparticles and may be assigned to the (110), (-113), (-122), (013), (031), (-202), (014), (224) Miller indices. The formed particles are compatible to the monoclinic silver sulfide Ag_2S from literature review [22]. The crystal structure of the samples has changed from the cubic phase of cadmium sulfid to monoclinic silver sulphide with increasing Ag⁺ions concentrations.
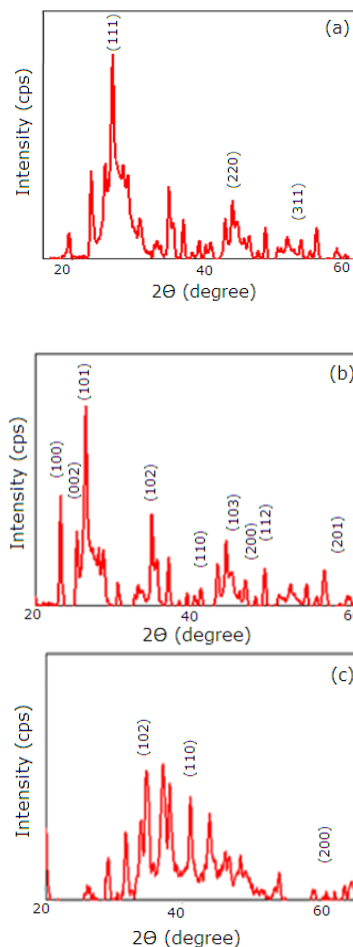
Figure 1. XRD patterns of CdS nanoparticles (a), Sample 1(b) and Sample 2 (c).

The size of the synthesized cadmium sulfide nanoparticles are calculated using Scherrer equation:

$$D = 0.9\,\lambda\,/\,\beta\,cos\theta$$

Whereλ represents wavelength ofX-rays, β represents half width at full maximum and θ is the diffraction angle [1]. Based on Scherer equation the average size of the particles are approximately 28 nm, 33 nm, 24 nm according to nanoparticles of CdS, sample1 and sample2.

In the ion exchange process, the decreasing of the particles size with the increase in concentration is related to the contraction of the particle area due to the increasing of transformation process. The localization of the particles decreases with increasing concentration of ion exchange process.

20

3.2. UV-vis spectroscopic analysis

The band gap of the synthesized cadmium sulfide nanoparticle and ion exchanged samples were determined by using UV-visible studies. The absorbtion spectra of obtained CdS powder and both of ion exchanged samples are shown in Figure 2.

In Figure.3 shows the graph to find the band gap of nanoparticles. From the graph, the optical band gap of cadmium sulfide nanoparticles is 2.25eV. The band gaps of ion exchanged samples are 1.62eV and 1.60eV according to Sample 1 and Sample2.
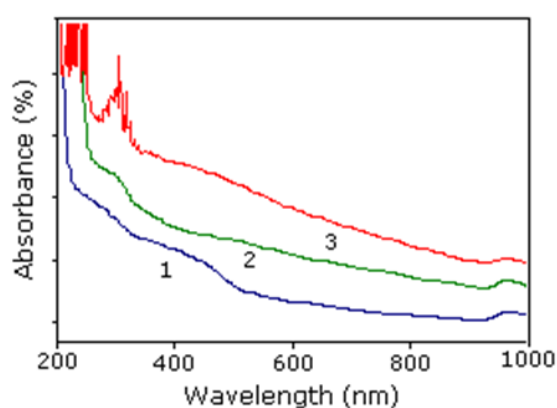
Figure 2.Absorption spectra of CdS nanoparticles (1), Sample 1(2) and Sample 2 (3).
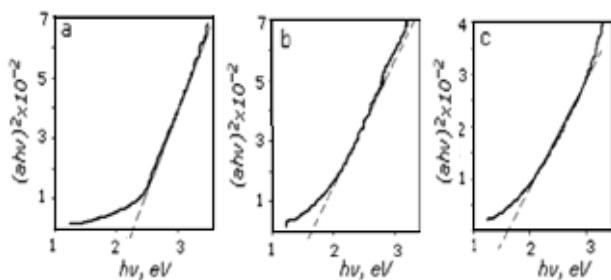
Figure 3. Band gap of CdS nanoparticles (a), Sample 1(b) and Sample 2 (c).

The direct band gap of CdS nanoparticles is 2.42 eV at room temperature [17]. Ag_2S is an effective semiconductor material due to a large absorption coefficient and a direct band gap of 0.9 eV to 1.05 eV [18]. With the increasing of the concentration, the value of the band gap zone has been reduced. After ion exchange process, the intermediate value of the band gap zone shows that two structures were formed: CdS and Ag_2S.

Comparing the value of the band gap by the particles size of calculated according to the XRD results, value of the band gap had to be increased by the reduction of the particles size, based on the quantum measurement effect. This is due to the different method of measurement. XRD allows that to define the size of the formed crystal structure.

3.3. Fourier Transform Infrared (FTIR) Spectroscopy

The Fourier Transform Infrared Spectroscopy (FTIR) was carried on CdS-MPA nanoparticles (a), Sample 1 (b) and Sample 2 (c) to identify the functional groups and the biomolecules. The FTIR results showed a number of absorption bands in the region 4000-400 cm^{-1}.
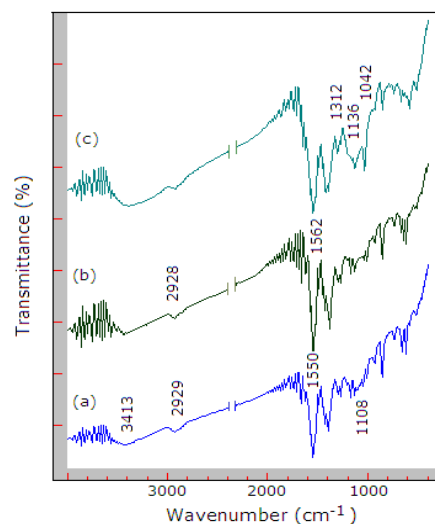
Figure 4. FTIR spectra of CdS nanoparticles (a),Sample 1(b) andSample 2 (c).

The peak in the range of 3413.6 cm^{-1}(a) and 3342.8 cm^{-1}(c) assigned to stretching vibration of hydroxyl group with strong hydrogen bond. Two strong peaks at 2929.5 cm^{-1} (a) and 2927.6 cm^{-1} (c) are the characteristic bands of the asymmetric and symmetric aliphatic C–H stretching vibration respectively. The characteristic infrared peak of C=C appeared at 1551.4 cm^{-1}(a) and 1550.2 cm^{-1}(c). The infrared absorption peak at 1108.3 cm^{-1}(a) and 1136.9 cm^{-1}(c) was assigned as C–C and C–O–C stretching vibrations. FTIR absorption spectra of the silver (CdS-Ag nanoparticles) occurring in the range of 1300-1000 cm^{-1}, peaks centered at 1312 cm^{-1}, 1201 cm^{-1},1136 cm^{-1}, 1042 cm^{-1} are due to the stretching vibrations of C-

21

O groups of anhydrides, esters, ethers, alcohols and phenols, C-O-H and of C-N of amines. The peak at 2313.7 cm^{-1} in (a) arises from the S-H stretching vibration of MPA. The Sample 1 (b) nanoparticles show a strong peak at 1562.3 cm^{-1} and 2928 cm^{-1}. Which corresponds to the C=C bending vibrations of aromatics and C-H stretching vibrations of alkanes.

3.4. Photoluminescence analysis of the CdS and ion exchange of CdS nanoparticles with Ag^{+}

The PL spectrum of samples was taken at room temperature in the range 200-1000 nm.The excitement wavelength was 385nm.At this time, samples were observed in the region of 400-600nm.In the radiation spectrum of the CdS aqueous solution, the blue-green region was observed to have a maximum of two luminescence: λ_{max}=527.95 nm and λ_{max}=486.96 nm.The PL spectrum of CdS nanoparticles are shown in Figure 5(a).
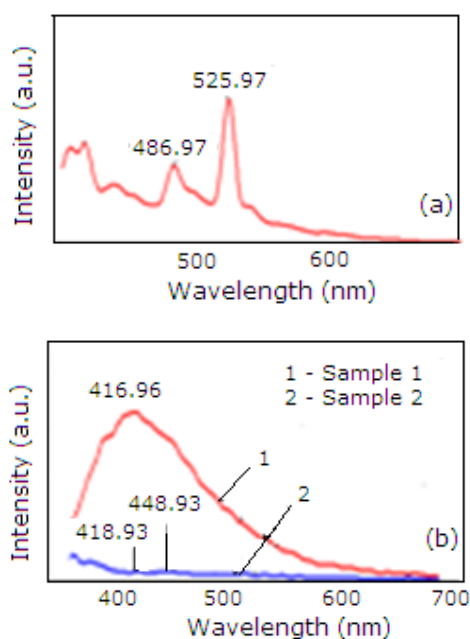
Figure 5. PL spectra of CdS nanoparticles (a),Sample 1 and Sample 2 (b).

Photoluminescence spectra were measured in the wavelength range 200-1000 nm excited at wavelength 330 nm [19]. Figure 5(b) shows the luminescence spectra of the ion exchange of sample 1 and sample 2. At the time, in the sample revealed violet-blue irradiation in the region of 380-500 nm [20, 21]. In the irradiation spectrum of the sample 1, the

maximum amplitude of the two luminescence was observed: λ_{max}=418.93nm and λ_{max}=448.93nm. There is an intensive radiation spectrum in the range of 350-450 nm with the increase in the molar concentration of the Ag$_2$S nanoparticles. At the same time, the observed irradiation line at λ_{max}=418 nm with the increase of concentration shifted towards the short wavelength region and observed at λ_{max}=416.96 nm.The observed red shift in the spectrum is associated with the broad of width of band gap zone of sample 2 compared with the sample 1.Thus, according to the spectrum, the band gap zone of sample 1and sample 2 were calculated as Eg = 2,95eV and Eg = 2,97eV, respectively.

4. CONCLUSION

The cadmium sulfid nanoparticles were synthesized by sonochemial method. The effects of the ion exchange process to structural, optical and photoluminescence properties of obtained particles were studied. In the ion exchange process with the increasing of concentration, the phase of the formed particles passed from the cubic phase of cadmium sulfid to monoclinic silver sulphide. From the FTIR spectrum, the stretching and bending frequencies of the molecular functional groups in the sample are studied.

5. REFERENCES

1. Alagar.M. et al./Int. J. Phy. Sci., 2011, v.6, p. 3662-3671.
2. HepziPramilaDevamani R. et al. / Elixir Nanotechnology, 2013, v. 61, p. 16917 – 16921.
3. Chen X. et al. / Chem. Rev., 2007, 107, p. 2891-2959
4. H. Fei. Y. et al./ Appl. Mater. Interfaces, 2010, v.2, p. 974-979.
5. Ma W. et al./ Nano Lett, 2009,v.9, p.1699-1703.
6. Won Y.-H. et al./ J. Mater. Chem., 2010, v.20, p. 5030-5034
7. Pan H. et al. / J. Phys. Chem. C, 2008, v.112, p.11227–11230.
8. Lin Y.F. et al. / Adv. Mater., 2008, v. 20, p. 3127–3130.
9. Shen G.Z. et al. /J Phys. Chem. B ., 2005, v. 109, p. 9294–9298.
10. Pal U. et al./ Thin Solid Films, 1997, v.305,

p.345-350.

11. Burda C. et al./ Chem. Rev., 2005, v.105, p.1025-1102.

12. Weller H./ Adv. Mater., 1993, v.5, p.88-95.

13. Gevko P. N. et al./Colloid J., 2016, v.78, p. 30–36.

14. Bulusheva L.G. et al./ Phys. Status Solidi B,2012, v.249, p. 2572-2575.

15. Okotrub A.V.et al./ Phys. Status Solidi B, 2013, v.250, p.2759-2764 .

16. Kenneth S. et al./ Phil. Trans. R. Soc. Lond. A (1999) 357, 335–353.

17. Arvind Kumar Vermaet al./ Research & Reviews: Journal of Material Sciences/ Volume 5 / Issue 2 / April, 2017, p.28-34.

18. Zamiri R. et al./ Chemistry Central Journal, 2015, v.9, p.28.

19. KapinusE. I. et al. / Zhurnalfizicheskoykhimii, 2011, v. 85, p. 748–752.

20. FakhriA.et al. / J. of Photochemistry and Photobiology B: Biology/,2015,p.1-19

21. XabaT..et al./Chalcogenide Letters, 2017,v.14, p. 37 – 346.

22. Gusev A.I. et al. / Semiconductors, 2016, v.50, p. 682–687.

SYNTHESIS OF BICYCLIC 1-AZAFAGOMINE ANALOGUE OBTAINED FROM DIETHYL (S)-3-(HYDROXYMETHYL)--3,6-DIHYDROPYRIDAZINE-1,2-DICARBOXYLATE

F.N.AXUNDOVA[1*], M.M.QURBANOVA[1], M.J.ALVES[2]

[1]Baku State University, Baku city, AZ-1073/1, Azerbaijan
[2]Organic Chemistry Department,Universidade do Minho Campus de Gualtar4710-057 Braga, Portugal

Pure (S)-(1,2,3,6-tetrahydropyridazin-3-yl) methanol was synthesized by a Diels-Alder cycloaddition using S-BINOL as a chiral inductor. The carbonylation of the hydroxyl group was led to form target bicyclic structure. The structures of synthesized compounds were proved by IR, 1H NMR, 13C NMR, HRMS (ESI) spectroscopies, and a specific rotation was determined by AUTOPOL III polarimeter.

1. INTRODUCTION

Aza sugars and imino sugars are subject to intense current interest.[1–3] A while ago it was found that a subtle change in the classical imino sugar inhibitor of nojirimycin type, by moving the nitrogen to the pseudo-anomeric position (the position that corresponds to the anomeric position in a monosaccharide), gave a very potent class of glycosidase inhibitors the so-called 1-azasugars.[4,5] An important class of glycosidase inhibitors is made up of thehydroxylated piperidines and pyrrolidines that occur in plants and microorganism and have been dubbed the "sugarshaped alkaloids from plants". They are reversible competitive inhibitors of glycosidases. One example of these compounds is l-deoxynojirimycin,which closely resembles glucose the ring oxygen has been exchanged for a nitrogen atom. A member of this class of compounds is 1-azafagomine , hydrazine, that inhibits both α- and β-glucosidase strongly. [6,7] The reason for the biological activity of 1-azafagomine is perhaps that, in the protonated form, it mimics the transition states of α-glucoside and β-glucoside cleavage. Recently, it was found out that 1-azasugars applied treatment of diabetes, [8] cancer, AIDS, [9]hepatit, [10] Gaucher,[10] tumor metastasis. Obviously, the field of iminosugars have become very exciting area for research on both chemical and biological fronts.

2. EXPERIMENTAL

Solvents were distilled under anhydrous conditions. All reagents were purchased and used without further purification. Glassware was dried prior to use. Compounds were purified by dry flash chromatography using silica 60, <0063 mm and water pump vacuum or by flash-chromatography using silica 60 Å 230–400 mesh as stationary phases. TLC plates (silica gel 60 F254) were visualized either at a UV lamp or in I2. 1H NMR and 13C NMR were run on a Bruker Avance III 400 spectrometers.((measuring frequency: 1H NMR = 400 MHz, 13C NMR = 100.6 MHz) Infrared spectra were recorded on a Bomem MB 104. Samples were run as oils as thin films. Melting points are uncorrected. MS spectra were recorded on a Varian 500-MS LC Ion Trap Mass and VG Autopsic M spectrometer. Specific rotation was determined by AUTOPOL III polarimeter.

Elemental analysis was performed on the analyzer Carlo Erba 1108.

NMR experiments

The NMR experiments have been performed on a BRUKER FT NMR spectrometer AVANCE 400 (Bruker, Karlsruhe, Germany) (400 MHz for 1H and 100.6 MHz for 13C) with a BVT 3200 variable temperature unit in 5 mm sample tubes using Bruker Standard software (TopSpin 3.1). The 1H and 13C chemical shifts were referenced to internal tetramethylsilane (TMS); the experimental parameters for 1H are as follows: digital resolution = 0.23 Hz,

24

SWH (spectral width in Hz) = 8224 Hz, TD (time domain) = 65 K, SI (Fourier transform size) = 32 K, 90 pulse-length = 10 μs, PL1 (power level for F1 channel) = 3 dB, ns (number of scans) = 1, ds (number of dummy scans) = 0, d1 (relaxation delay) = 1 s and for ^{13}C as follows: digital resolution = 0.27 Hz, SWH = 25253 Hz, TD = 65 K, SI = 32 K, 90 pulse-length = 9 μs, PL1 = 2 dB, ns = 100, ds = 2, d1 = 3 s.

HSQC: pulse program = hsqcetgp, digital resolution = 1.97 Hz, SWH = 5342, TD = 4096, SI = 1024, 90 pulse-length = 20 μs, PL1 = 3 dB, ns = 4, ds = 16, d1 = 1.5 s.

HMBC: pulse program = hmbcgplpndqf, digital resolution = 1.97 Hz, SWH = 6810, TD = 4096, SI = 2048, 90 pulse-length = 20 μs, PL1 = 3 dB, ns = 24, ds = 16, d1 = 1.5 s.

The NMR-grades DMSO-d_6, CDCl$_3$, CD$_3$OD, D$_2$O was used for the solutions of 1-7.

IR experiments

Infrared spectra were recorded on a Bomem MB 104. Samples were run as oils as thin films. The spectrum was taken in the range of 4000-400 cm^{-1} at room temperature.

MS experiments

MS spectra were recorded on a Varian 500-MS LC Ion Trap Mass and VG Autopsic M spectrometer.

Synthesis of (2*E*)-Penta-2,4-dien-1-ol

250 ml necked bottom flask with magnit stir bar was placed in ice bath, 5.09 g 2,4-pentadienic acid was dissolved in dried THF (77 ml) then NEt$_3$ 8.9 ml was added, 5 ml ethyl chloroformate dissolved in 13 ml THF and placed in dropping funnel then was connected with 250 ml three bottom flask and left it to pour drop by drop after that left it to stir for 30 min -5^0-0^0 C. After 30 min reaction was stopped and filtrated under the vacuum then was washed thoroughly THF (3×50ml) (Solution A). 1L three necked bottom flask was placed in ice bath (7^{0}C) 515 ml H$_2$O, 4.804 g NaBH$_4$ were added and was stirred (temperature 15-17^{0}C). Solution A was added drop by drop for 30 min, in meanwhile ice bath was removed then left it to stir for 3.5 h. In the next step after 3.5 h 1L flask was placed nine bath 20 ml 37% HCl was added (under N balloon) with dropping funnel drop by drop. The mixture was extracted firstly with diethyl ether (200 ml+2×100 ml) organic layer was combined washed with 10 % NaOH (50 ml) +

H$_2$O (50 ml) + Brine (50 ml) then MgSO$_4$ was added and filtrated under the vacuum. Using Buchi-580 under 75^{0}C temperature diethyl ether and THF were distillated to obtain 2,4-pentadienol.], ν_{max} (CHCl$_3$)/cm^{-1} 3616, 3444, 2873, 2254, 1824, 1731, 1606, 1455, 1377, 1083, 994, 902; δ_H (400 MHz; CDCl$_3$) 6.25 (2H, m, CH$_2$=CH), 5.74 (1H, dt, J=14.7, 5.7, CH=CH$_2$OH), 5.13 (1H, d, J=16.4, CH), 5.01 (1H, d, J=9.6, CH), 4.07 (2H, m, CH$_2$OH), 3.12 (1H, br s, OH); δC (100 MHz; CDCl$_3$) 136.2 (CH), 132.5 (CH), 131.2 (CH), 116.9 (CH$_2$), 62.3 (CH$_2$).Anal. Calcd.for C$_5$H$_8$O: C, 71.42; H, 9.52. Found: C, 71.47; H, 9.48.

Synthesis of (S)-Diethyl 3-(hydroxymethyl) pyridazine-1,2(3H,6H)-dicarboxylate (1)

Solution A was diluted with dry toluene (10 mL), added to solution B, stirred for 5 min, and then refrigerated at -78 ºC. To this mixture was added a solution of diethyl azodicarboxylate (543 μL; 1.19 mmol) in dry toluene (10 mL). The temperature was allowed to rise gradually to rt, and the reaction mixture was stirred for 18h. The reaction was quenched with saturated solution of NaHCO$_3$ (1 mL), filtered through a pad of Celite®, and the Celite® washed with EtOAc (3 × 20 mL). The filtrates were combined and concentrated under reduced pressure giving a yellow oil. The crude oil was purified by "dry-flash" chromatography (silica, petroleum ether / diethyl ether). (S)-BINOL was recovered with petroleum ether (1): ether (1) (0.200 g; 69%) and product (-)-**1** with diethyl ether (0.225 g; 73%) as a yellow oil.

Solution A: a solution of Me$_2$Zn 1.2 M in toluene (991 μL; 1.19 mmol) was added to a solution of penta-2,4-dien-1-ol (0.100 g; 1.19 mmol) in dry toluene (6 mL) at 0 ºC, and stirred for 5 min.

Solution B: a solution of MeMgBr 1.4 M in toluene/THF (849 μL; 1.19 mmol) was added to a solution of (S)-BINOL (0.340 g; 1.19 mmol) in dry toluene (6 mL) at 0 ºC, and stirred for 5 min.

$[\alpha]_D^{20}$ -23.4º (conc. 1.25% in CHCl$_3$). ν_{max} (neat) 3483, 1707 cm^{-1}. δ_H (400 MHz, CDCl$_3$) 1.23-1.30 (12H, m, 4 × CH$_3$, A+B), 2.58 (1H, br s, OH), 3.35 (1H, dd, J 12.3, 9.5 Hz, H-3', A), 3.45 (1H, dd, J 12.0, 9.8 Hz, H-3', B), 3.56-3.69 (2H, m, 2 ×H-3', A+B), 3.77 (1H, dd, J 13.5, 4.3 Hz, H-6, A), 3.91 (1H, br s, H-6, B), 4.11-4.26 (8H, m, 4 × CH$_2$, A+B),

4.30 (1H, tdd, J 6.0, 3.9, 2.2 Hz, H-6, B), 4.34-4.44 (1H, m, H-6, A), 4.72 (2H, br s, H-3, A+B), 5.66-5.88 (4H, m, H-4 + H-5, A+B) ppm. δ_C (100 MHz, CDCl$_3$)[19] 14.3 (CH$_3$, A), 14.4 (CH$_3$, B), 42.2 (C-6, A), 43.6 (C-6, B), 55.9 (C-3, A), 56.9 (C-3, B), 61.9 (C-3', A+B), 62.6, 62.7, 62.8, 62.9 (CH$_2$, A+B), 123.4, 124.2, 124,6, 125.2 (C-4 or C-5, A+B), 154.9, 155.7, 156.2, 156.3 (C=O, A+B) ppm. HRMS (ESI): calcd for C$_{11}$H$_{18}$N$_2$NaO$_5$: 281.1108; found: 281.1109.

Ssynthesis(S)-(1,2,3,6-tetrahydropyridazin-3-yl) methanol (2)

To a stirred solution of cycloadduct1 (0.119 g; 0.461 mmol) in THF (2 mL) was added NaOH 2M (2mL). The mixture was left under reflux for 3h. After cooling down to the reaction mixture was added THF (2 mL), and a suspension of Amberlite (H$^+$) in water. The mixture was swirled o promote contact and then immediately filtrated under the vacuum. The solvent was evaporated. By adding acetone, water was co-evaporated in the rotary evaporator giving a yellow oil (0.048 g; 91.0 %). $[\alpha]_D^{20}$ -20º (conc. 0.3% in EtOH). ν_{max}(neat): 3422 (N-H), 1643 (C=C) cm^{-1}. δ_H (400 MHz, D$_2$O) 6.01 (1H, ddd, J 2.4, 5.6, 10.4 Hz H-5), 5.79 (1H, ddd, J 2.0, 4.4, 10.4 Hz, H-4), 3.65-3.57 (2H, m, H-3'), 3.54-3.48 (1H, m, H-3), 3.35 (1H, ddd, J 2.8, 5.2, 17.6 Hz H-6), 3.24 (1H, ddd, J 2.6, 3.2, 17.2 Hz, H-6) ppm. δ_C(100.6 MHz, D$_2$O) 127.4 (C-4 or C-5), 125.0 (C-5 or C-4), 62.5 (C-3'), 54.8 (C-3), 44.2 (C-6) ppm. HRMS (ESI): calcd for C$_5$H$_{10}$N$_2$O [M+H]$^+$ 114.0793; found: [M+H]$^+$ 115.0165.

Synthesis of (5S)-3-oxa-1,9-diazabicyclo [3.3.1] non-6-en-2-one (3)

To stirred solution of **2** (0.051g; 0.447 mmol) dissolved in DCM (4.6ml) (dried) were added DIPEA (10 ekv, 0.78 ml; 0.447 mmol) and triphosgene (0.5ekv, 0.066g; 0.447mmol) then left to stir for 5 min at the rt. The solvent was removed. The column was applied (2:1 EtOAc: Petr/ether) to obtain yellow oil (0.0031g; 7%)ν_{max}(neat): 3289,2924 (N-H), 1714 (C=O) cm^{-1}. (400 MHz, CDCl$_3$) 6.11 (1 H, ddt, J 10.0, 6.8, 1.2 Hz , H$_D$ and H$_C$), 5.84 (1H, m, H$_D$ or H$_C$), 4.60 (1H, dd, J 10.4, 6.4, H$_F$ or H$_G$, CH$_2$-O), 4.45 (2H, dd, J 10.08 Hz, H$_F$ or H$_G$, CH$_2$-O, NH), 4.05 (1H, ddd, J 17.2, 4.0, 1.2 H$_2$, CH$_2$N), 3.88 (1H ,ddd, J 17.2, 4.0, 1.6 H$_2$, CH$_2$N), 3.81 (1H, br d, J

5.6 H$_2$, H$_E$) ppm. δ_C(100.6 MHz, CDCl$_3$), 130.2 (CH), 125.3 (CH), 74.3 (CH$_2$O), 52.4 (CH$_2$N), 45.5 (CH) ppm

3. RESULT AND DISCUSSIONS

Optically pure (S)-Diethyl 3-(hydroxymethyl) pyridazine-1,2(3H,6H)-dicarboxylate (1) was obtained according to Bols's protocol [11] by changing the dienophile /diethyl azodicarboxylate (DEAD) instead of 4-phenyl-1,2,4-triazole-3,5-dione (PTAD) and using chiral catalyst BINOL. 2,4-Pentadienol was obtained by repeating the literature procedure. [12] The main reason to choose Diels-Alder strategy to reach (1) is that it would be quite a short route. Cleavage of ethyl carbamate groups under reflux of an aqueous solution of NaOH 2M/dioxane for 3h followed by treatment with the acidic resin leading to pure (S)-(1,2,3,6-tetrahydropyridazin-3-yl) methanol (2) in 99% yield. The structures of compound (2) were confirmed by 1H and 13C NMR, IR, and HRMS analysis. Specific rotation for compound (2) was determined by AUTOPOL III polarimeter.
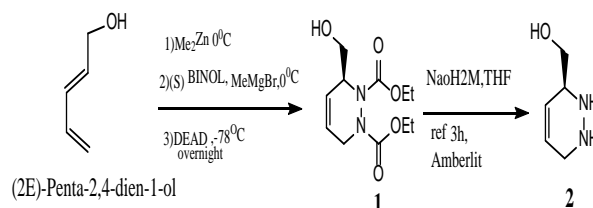
Scheme 1. The synthesis of azafagomine analogue based on optically active cycloadducts
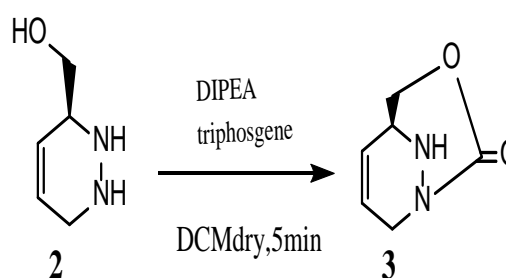
Scheme 2. The synthesis of azafagomine analogue

The treatment (2) with bis(trichloromethyl)-carbonate (triphosgene)[11] in the presence diisopropylethylamine (DIPEA) gives the product (3) in just 5 minutes after purification with column chromatography.

4. CONCLUSION

In conclusion, pure (S)-(1,2,3,6-tetrahydropyridazin-3-yl) methanol was synthesized based on (S)-Diethyl 3-(hydroxymethyl) pyridazine-1,2(3H,6H)-dicarboxylate (1) in high yield. The obtained compound was used to obtain optically active 1-azafagomine analogues.

5. REFERENCES

1. Heightman T. D. et al./AngewandteChemie International Edition,1999,v. 38, p.750.
2. Zechel D.L.et al./AmericanChemicalSociety, 2000,v. 33, p.11.
3. StützetA. E. al./Iminosugars as Glycosidase Inhibitors: Nojirimycin andBeyond, 1999.
4. M. Bols et al./Accounts of Chemical Research,1998, v. 31, p.1-8
5. Ichikawa Y. et al./AmericanChemicalSociety 1998, v. 120, p. 5854.
6. BolsetM.al./European Journal of Organic Chemistry 1997, №6, p. 940–947.
7. Bols M. et al./European JournalofChemistry 2000, v. 6, p. 278.
8. KarpasetA al./Pro,"virl Arad. SCI. L'. S. A.1988, v. 85, p.9229-9233.
9. Jacob G.S..et al./"Natural Products as Antiviral Agent" 1992, pp. 137-152.
10. AlperetJ. al./Carbohydrate Chemistry, 2001, v. 291, pp.2338.
11. BolsM. et al European Journal of Chemistry. 2000, v. 6, pp. 278–287.
12. Petty P. J. et al. / In Organic Syntheses, Coll, Organic Syntheses. 1988, v. 6, p. 95-98

RESEARCHING ANTIMICROBIAL PROPERTIES OF DICHLORO DIAZABUTADIENE SYNTHESIZED BASED ON 4-CHLOROBENZALDEHYDE

G.T.SULEYMANOVA[1], Kh.N.BAGİROVA[1], D.S.GAFAROVA[2], G.V.BABAYEVA[3], S.H.MUKHTAROVA[1], N.F.MIKAYILOVA[1], L.R.HUSEYNOVA[1], N.G.SHIKHALIEV[1*]

[1]Organic Chemistry Department, Baku State University, Z.Khalilov 23 Str., Baku, Azerbaijan
[2]General and Toxicological Chemistry Department, Azerbaijan Medical University, Semed Vurgun str, Bakı, Azerbaijan
[3]Analytical and Organic Chemistry Department, Azerbaijan State Pedagogical University, Uzeyir Hajibeyli 68str. Baku, Azerbaijan

Antimicrobial properties of 1.1-dichlorodiazene derivatives synthesized from phenylhydrazones which have high physiological activity have been researched against gram-positive golden staph (*St.aureus*), gram-negative bacilli (*E.coli*), pigment producing blue-green pus (*Ps.aeruginoza*) and candida fungus *(C.albicans)*. Antibacterial and antifungal properties of synthesized substanceswere approved according to results.

1. INTRODUCTION

It is evident that, phenylhydrazones are easily synthesized substances which have high pharmacological properties. They are the main part of antimicrobial, anti cold, anticancer, antifungal, anti tuberculosis, antivirus and antimalarial medicines [1-8]. Schiff bases of phenylhydrazone are also used as useful sintons for synthesizing N-heterocyclic substances (pyrazoles, pyridazine, dehydropyridazine etc.) which have high biological activity.

In a presence of CuCl-catalyzed olefination of 1.1-dichlorodiazene derivatives synthesized from phenylhydrazones which are physiologically active, have received research interest [9-16]. So, biological activity of (E)-1-(2,2-dichloro-1-phenylvinyl)-2-phenyldiazene synthesized at previous research was examined and determined that, this substance has antibacterial and antifungal properties [17].

2. EXPERIMENTAL PART

Thus, dichlorodiazenes of corresponding phenylhydrazones which are synthesized from Cl derivatives of benzoy aldehyde were synthesized, respectively, their antimicrobial properties were determined according to the serial dilution method.
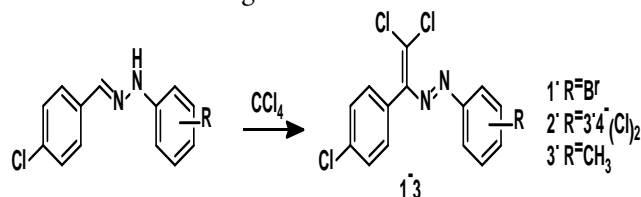
1. (E)-1-(4-bromophenyl)-2-(2,2-dichloro-1-(4-chloro-phenyl)ethyl) diazene
2.(E)-1-(2,2-dichloro-1-(4-chlorophenyl)ethyl)-2-(3,4-dichlorophenyl) diazene
3.(E)-1-(2,2-dichloro-1-(4-chlorophenyl)et-hyl)-2-(p-tolyl)diazene

For this, 1% solution of a new substance into ethanol was diluted into sterile distilled water at 1:100, 1:200, 1:400, 1:800 ratios, (1,2,3,4).

Antimicrobial property of these substances was researched in compare with ethanol, nitrofungin and rivanol. As test-cultura, gram-positive golden staph (*St.aureus*), gram-negative bacilli (*E.coli*), pigment producing blue-green pus (*Ps.aeruginoza*) and Candida fungus *(C.albicans)*were taken. To grow bacteria meat peptone agar, to grow fungus Saburo food enviroment was used.

Growings were done in each 10, 20, 40 and 60 minutes, for bacterias they were kept 24 hours at 37

28

degree Celsius, for fungus they were kept 48 hours at 28 degree Celsius.

In this experiment, emultion of 500 million microbe in 1 ml was dropped into each vial. Growing was done from each vial after 10, 20, 40 and 60 minutes. Obtained new substances and antimicrobial properties of controlls are given in the following table.

3. CONCLUSION AND DISCUSSION

As it is shown in a table, all of 3 new obtained substances have antimicrobial effect, but to different microbes, these substances differ from each other. (E)-1-(2,2-dichloro-1-(4-chlorophenyl)ethyl)-2-(3,4-dichlorophenyl) diazen is more active within these substances.

But, in comparison bacillus had stood, this means that, in this ratio that substance had killing effect in every hour.

(E)-1-(2,2-dichloro-1-(4-chloro-phenyl) ethyl)-2-(3,4-dichlorop henyl)diazen even in a 1:800 ratio killed staphylococks in one hour.

(E)-1-(2,2-dichloro-1-(4-chloro-phenyl) ethyl)-2-(p-tolyl)diazene killed blue-green pus in a ratio 1:400 in one hour, those 4 sort of microorganisms during 20 minutes in a ratio 1:100.

(E)-1-(4-bromophenyl)-2-(2,2-dich-loro-1-(4-chlorophenyl)ethyl)diazene had stopped growth of all of these microbes for 10 minutes in a ratio 1:200, but had killed candida during 60 minutes in a ratio 1:800.

Table 1. Antimicrobial effect of new syntesized substances-
(Symbols: 1, 2, 3, 4 are properly
1:100, 1:200, 1:400, 1:800 ratios, "+":
process fully completed, "–": process
did not complete.

Test culturas	Exposition time (minute)	Inspected items 1				Inspected items 2				Inspected items 3			
		1	2	3	4	1	2	3	4	1	2	3	4
St.aureus	10	-	-	+	+	-	-	+	+	-	+	+	+
	20	-	-	+	+	-	-	-	+	-	-	+	+
	40	-	-	+	+	-	-	-	+	-	-	+	+
	60	-	-	-	+	-	-	-	-	-	-	+	+
Ps.aeruginoza	10	-	-	+	+	-	-	+	+	-	+	+	+
	20	-	-	+	+	-	-	+	+	-	-	+	+
	40	-	-	+	+	-	-	-	+	-	-	+	+
	60	-	-	+	+	-	-	-	+	-	-	-	+
E.coli	10	-	-	+	+	-	-	+	+	-	+	+	+
	20	-	-	+	+	-	-	+	+	-	-	+	+
	40	-	-	+	+	-	-	+	+	-	-	+	+
	60	-	-	+	+	-	-	+	+	-	-	+	+
Candida albicans	10	-	-	+	+	-	-	+	+	-	+	+	+
	20	-	-	+	+	-	-	+	+	-	-	+	+
	40	-	-	+	+	-	-	-	+	-	-	+	+
	60	-	-	-	+	-	-	-	+	-	-	+	+

So, this substance killed staphylococks during 20 minutes, blue-green pus and Candida during 40 minutes in a ratio 1:400.

Table 2. Antimicrobial properties of controlls

Controlls Rivanol				Ethanol				Nitrofungin			
1	2	3	4	1	2	3	4	1	2	3	4
+	+	+	+	_	+	+	+				
+	+	+	+	_	+	+	+				
+	+	+	+	_	+	+	+				
-	-	+	+	-	+	+	+				
+	+	+	+	+	+	+	+				
+	+	+	+	_	+	+	+				
+	+	+	+	_	+	+	+				
-	-	-	+	_	+	+	+				
-	-	-	+	+	+	+	+				
-	-	-	+	-	+	+	+				
-	-	-	+	_	+	+	+				
-	-	-	+	_	+	+	+				
+	+	+	+	+	+	+	+	+	+	+	+
+	+	+	+	+	+	+	+	+	+	+	+
+	+	+	+	-	+	+	+	-	+	+	+
+	+	+	+	-	+	+	+	-	+	+	+

4. CONCLUSION

Thus, according to the bactericide and fungicide activity, (E)-1-(2,2-dichloro-1-(4-chlorophenyl)ethyl)-2-(3,4-dichlorophenyl) diazene) can be shown as the most effective substance among the substances which were researched in microbiological laboratory and this substance can be recommended as an antimicrobial substance

29

5. ACKNOWLEDGMENTS

6. REFERENCES

1. Fekri, Roghayeh; et al/ Inorganica Chimica Acta, 2019, v. 484, p. 245 – 254.
2. Lapasam, Agreeda et al/ Inorganica Chimica Acta, 2019, v. 484, p. 255 – 263.
3. Palepu, NarasingaRao et al/ / Arabian Journal of Chemistry, 2018, v. 11, 5, p. 714 – 728.
4. Fekri, Roghayeh; et al/ Applied Organometallic Chemistry, 2018, v. 32, 2.
5. Bakale, Raghavendra P.; et al/ Journal of Molecular Structure, 2018, v. 1154, p. 92 – 99.
6. Ajani, Olayinka O. et al/ Journal of Heterocyclic Chemistry, 2018 vol. 55,1,p. 302 – 312.
7. Nagula, Narsimha; et al/ Journal of Fluorescence, 2018, v. 28, 1, p. 225 – 241.
8. Knittl, Esther Theresa et al / Monatshefte fur Chemie, 2018, v. 149, 2, p. 431 – 443.
9. Nenajdenko V.G.et al. /ACS Catal, 2017, v. 104, 3, p.1-6 – 672.
10. Shikhaliyev. N. Q. et al./Dyes and Pigments, 2018, v. 150, p. 377–381.
11. MaharramovA.M.. et al. Dyes and Pigments/ v. 159, 2018, p 135-141.
12. Shikhaliev N.Q. et al./ News of Baku University, 2016, №1, p.40-49.
13. Shikhaliev N.Q. et al./ News of Baku University, 2016, №3, p.5-12
14. MaharramovA.M..et al.Chemical Problems Journal, 2018, №2, p-230-238.
15. Maharramov A.M. et al./ Journal of Low Dimensional Systems, 2018, v. 2 (1), p-37-44.
16. Shikhaliev N.Q. et al./Journal of Low Dimensional Systems, 2018, v. 2 (2), p-24-29.
17. Maharramov A.M. et al./ Journal of Low Dimensional Systems, 2017, v.1 (1), p.4-7

MULTICOMPONENT CASCADE CARBOCYCLATION REACTION ON THE BASIS OF METHYLENE ACTIVE NITRILES, BENZALDEHYDE AND ACETYLACETONE

A.I. ISMIYEV*, N.M.JABBARLI

Baku State University, Z.Khalilov Str. 23, Baku, Azerbaijan

The interaction of representatives of methyleneactive nitriles such as malononitrile and butyl 2-cyanoacetate with benzaldehyde and acetylacetone was studied and it was determined that the structure of nitrile component and the sequence of adding of the reagents into the reaction medium affected significantly to the reaction course. Thus, the reaction of benzaldehyde, malononitrile and acetylacetone respectively in a molar ratio of 2:2:1 in the presence of NaOH as catalyst results in the synthesis of new bicyclic system– 3-aza-7-acetyl-4-imino-2-oxo-6-methyl-1,5-dician-8,9-diphenylbicyclo[3.3.1]nonen-6 compound. The multicomponent interaction of the butyl 2-cyano-acetate with the same reagents led to the formation of dibutyl 1,3-dician-2,6-diphenyl-5-acetyl-4-hydroxy-4-methylcyclohexane-1,3-dicarboxylate. The structure of the synthesized compounds was confirmed by X-ray analysis.

1. INTRODUCTION

One of the developed trends of modern organic chemistry in recent years is related with the preparation of productive methods for the synthesis of complex carbo-, heterocyclic compounds. The effectiveness of these methods is provided through creation of synthesis schemes with minimal stages, total convergent, minimal consumption of reagents, solvents and other material resources. The obtaining of starting substances in easy manner is also an aspect that increases the efficiency factor. From the point of view of the strategies developed in modern times,it is necessary to mention the multicomponent reactions that are entered into the synthetic arsenal of organic chemistry. Multicomponent reactions are carried out in a single reactor on the basis of interaction of at least three substances, reaction products contain structural fragments of starting substances,added reagents simultaneously constitute the final product through consistent happening elementary transformations (cascade or tandem reactions)[1-4].

Methylene active nitriles (malononitrile, malonodinitrile, alkyl 2-cyanoacetates and etc.) are one of the bifunctional reagents that perform as sintone of various multicomponent reactions, generate multi vectorial transfor-mations [5-9] and the chemistry of these compounds has not yet fully expended its synthetic potential.

2. EXPERIMENTAL

The aim of the current reseach has consisted to determine the new directions of the inter-action of benzaldehyde, butyl 2-cyanoacetate and acetylacetone. The reaction of these reagents usually results in formation of 2-amin opirane compounds and there are research works in the literature confirming this [10-15].As a result of investigations, it was determined that adding of benzaldehyde (I), butyl 2-cyanoacetate (II) and acetylacetone (III) in certain sequence in the presence of base catalyst NaOH led to the formation of previously unknown carbocyclation product-dibutyl 1,3-dician-2,6-diphenyl-5-ace-tyl-4-hydroxy-4-methylcyclohexane-1,3-dicar-boxylate (IV) with 66% yield(Scheme 1.):
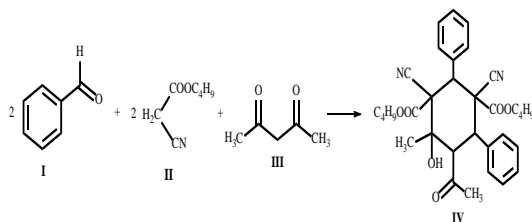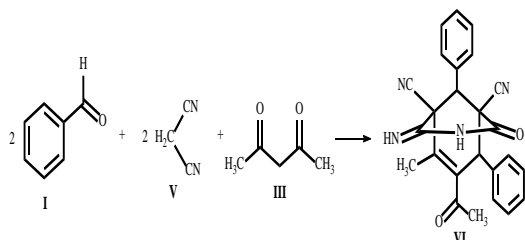
Scheme 1. The synthesis of compound IV

In order to confirm the structure of synthesized compound (IV)was applied to^{1}H and ^{13}C NMR spectroscopy methods.Signals corresponding to proton and carbon atoms in NMR spectra were observed. However, due to the fact that spectroscopic data were not enough for structure confirmation, X-ray analysis was done, which allowed totally confirm the structure of investigated compound.

The single crystal of compound (IV)was obtained by two times recrystallization from ethanol.

The interaction of benzaldehyde (I), acetyl-acetone (III) and malononitrile (V) in the same molar ratio and under the similar condition resulted in the synthesis of 3-aza-7-acetyl-4-imino-2-oxo-6-methyl-1,5-dician-8,9-diphenyl-bicyclo[3.3.1]nonen-6 (VI)with 72% yield(Scheme 2.):

Scheme 2. The synthesis of compound VI

The structure of compound (VI) was also confirmed by X-ray analysis method.

The synthesis of dibutyl 1,3-dician-2,6-diphenyl-5-acetyl-4-hydroxy-4-methylcyclo-hexane-1,3-dicarboxylate(IV)

10 ml of ethanol, 0.53g of benzaldehyde (5 mmol) and 1.41g(10 mmol) of butyl 2-cyanoacetate were placed to 50ml flat flask supplied with magnetic mixer. In mixing condition Afterwards, 3ml of water solution of 0.1g of NaOH was added to

the reaction medium. After half an hour, 0.5g of acetylacetone (5 mmol) and 0.53g of benzaldehyde (5 mmol) were added to the medium. The reaction medium was kept at room conditions for 48 hours after mixing for one more hour. The precipitated crystals were filtered and recrystallized in ethanol.

The synthesis of 3-aza-7-acetyl-4-imino-2-oxo-6-methyl-1,5-dician-8,9-diphenylbicyclo[3.3.1]nonen-6(VI)

20 ml of ethanol, 0.53g of benzaldehyde (5 mmol) and 0.66g of malononitrile (10mmol) were placed to the 50ml flat flask supplied with magnetic mixer. Afterwards, 5ml of water solution of 0.2g of NaOH was added to the reaction medium. After half an hour, 0.5g of acetylacetone (5 mmol), 0.53g of benzaldehyde (5 mmol) were added to the medium. The reaction medium was kept at room conditions for 24 hours after mixing for one more hour. The precipitated crystals were filtered and recrystallized in ethanol.

3. RESULTSAND DISCUSSION

^{1}H and ^{13}C NMR spectra recorded on a Bruker AC-300 instrument (300 MHz on 1H and 75 MHz nuclei at 13C cores) in a $(CD_3)_2SO$ solution, residual signals of the solvent used as the standard. The melting points were determined on a Kofler's table. TLC monitored the purity of the resulting compounds on Silufol UV-254 plates, eluent acetone-hexane 1:1, developer-iodine vapor, UV detector.The XRD analysis of compounds **IV**and **VI** were performed on a Brucker SMART APEX II CCD diffractometer (MoK_α radiation, graphite monochromator, φ- and ω-scanning).

Crystal data: $C_{33}H_{38}N_2O_6$, M 558.65, ortho-rhombic, space group Pbca, a=14.1473(7) Å, b =16.2061(9) Å, c =25.3549(14)Å, α= 90º, β= 90º, γ=90º, V = 5813.2(5) Å^3, Z =8 , d$_c$ = 1.277 mg/m^3, μ = 0.088 mm^{-1}, F(000) = 2384, crystal size 0.233 × 0.227 × 0.226 mm^3. The intensity data were collected within the range of 1.606≤θ≤ 27.000° using Mo-K$_\alpha$ radiation (λ = 0.71073 Å). Reflection

collected-66196; independent reflections-6106[R(int)= 0.0734]; completeness to theta=25.242º - 97.6%; final R indices [I>2sigma(I)] – R1=0.0613, wR2=0.1328; R indices (all data) - R1=0.0803, wR2=0.1404. All calculations were carried out using the SHELXTL program package[16]. Crystal data: $C_{27}H_{26}N_4O_3$, M 454.52, monoclinic, space group $P2_1/n$, a=13.6759(8) Å, b =9.5691(6)Å, c =19.1533(12)Å, α= 90º, $β$= 97.090(2)º, γ=90º, V = 2487.3(3) Å3, Z =4 , d_c = 1.214 mg/m^3, μ = 0.081 mm^{-1}, F(000) = 960, crystal size 0.343 × 0.270 × 0.176 mm^3.
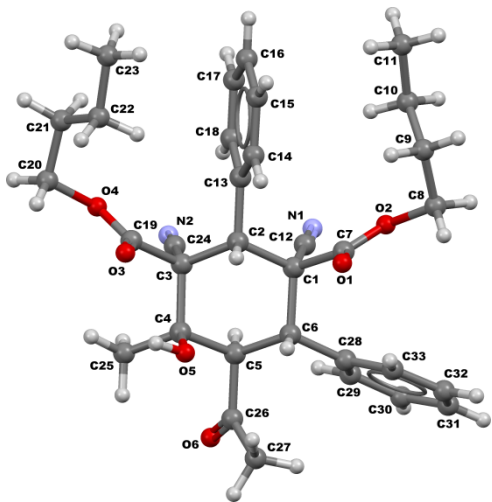

Figure 1. The monocrystalline of compound (IV)
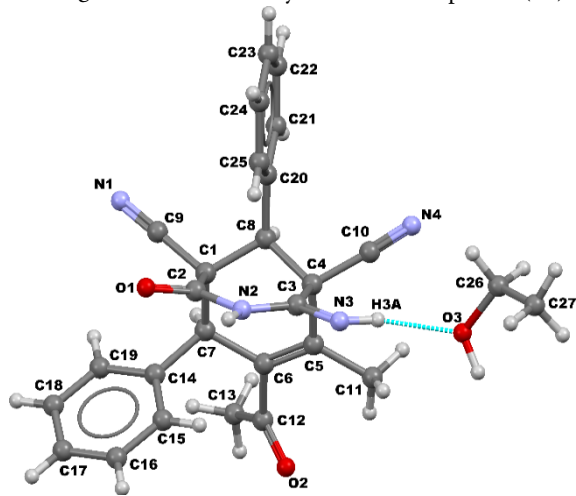
Figure 2. The monocrystalline of compound(VI)

The intensity data were collected within the range of 1.733 ≤θ≤ 25.999° using Mo-K$_α$ radiation (λ = 0.71073 Å). Reflection collected-23861; independent reflections- 4751[R(int)= 0.0915]; completeness to theta=25.242º - 98.4%. All calculations were carried out using the SHELXTL program package[16].

Dibutyl 1,3-dician-2,6-diphenyl-5-acetyl-4-hydroxy-4-methylcyclohexane-1,3-dicarboxy-late(IV), colorless solid, $t_{m.p}$ =205^{0}C yield: 66%

^{1}H NMR (300 MHz, (CD$_3$)$_2$SO)),δ,m.h.: 0,98 (6H, t,CH$_3$); 1.10 (3H, s, CH$_3$); 1,20-1,30 (8H, m,CH$_2$); 2,1 (3H, s, CH$_3$); 2.7 (1H, d, CH$_3$); 3.6(1H, d, CH); 4.21 (4H, kv, OCH$_2$); 7.19-7.29 (10H, m, CHar)

^{13}C NMR (75 MHz, (CD$_3$)$_2$SO)): 14.1; 14.3; 21.3; 32; 41.5; 46.7; 48.8; 54.8; 60.7; 61.3; 62; 70; 110.1; 110.2; 126.4; 126.5; 128.5; 129.0; 137.6; 144; 168.0; 170; 210

3-aza-7-acetyl-4-imino-2-oxo-6-methyl-1,5-dician-8,9-diphenylbicyclo[3.3.1]nonen-6(VI), bright yellow solid, $t_{m.p}$ =295^{0}C yield: 72%

^{1}H NMR (300 MHz, (CD$_3$)$_2$SO, δ, ppm): 2.1 (3H, s, CH$_3$); 2.18(1H, s, CH$_3$); 4.56 (1H, s, CH); 5.04 (1H, s, CH); 7.1-7.5 (10H, s, Car); 9.36 (2H, s,NH)

13C NMR (75 MHz, (CD$_3$)$_2$SO, δ, ppm): 18.0 (CH3); 26 (CH3); 42.0 (CH); 44.68 (CH); 60.0 (OCH2); 62.0(C); 113 (CN); 115 (CN); 130.54 (CHar); 131.0 (CHar); 129.2 (CHar); 137.0(Car); 158.66 (CON); 164 (C=NH); 198.0 (C=O)

4. CONCLUSION

In conclusion, we can say that new transformations -cascade carbocarbocyclation and heterobicarbocyclation directions were determined duringinteraction ofbenzaldehyde and acetylacetone with methyleneactive nitriles.

5. REFERENCES

1. Simon S., Contantieux T., Rodrigues J. Utilisation of 1,3-dicarbonyl derivatives in multicomponent reactions// Eur. J.Org. Chem.,

2004, No24, pp. 4957-4980.

2. Hugel H. Microwave multicomponent synthesis// Molecules, 2009, v.14, No12, pp.4936-4972.

3. Ganem B. Strategies for innovation in multicomponent reaction design// Acc.Chem. Res., 2009, v.42, No3, pp.463-472.

4. Eckert H. Diversity oriented synthesis of conventional heterocycles by smart multicomponent reactions (MCRs) of the last decade// Molecules, 2012,v.17., No 9, pp.1074-1102.

5. Shestopalov A.M., Shestopalov A. A., Rodinovskaya L.A.Multicomponent reactions of carbonyl compounds and derivatives ofcyanoacetic acid: synthesis of carbo- and heterocycles // Synthesis, 2008, No1, pp.1–25.

6. Wang K., Kim D., Domling A. Cyanoacetamide MCR (III): three-com-ponentGewald reactionsrevisited // J. Comb. Chem.2010,v.12, No1, pp.111–118.

7. Shaabani A., Hooshmand S.E. Malononitrile dimer as a privileged reactant in design and skeletaldiverse synthesis of heterocyclic motifs// Molecular Diversity, 2018, v.22, No1, pp.207-224.

8. Ismiyev A.I., Hajiyeva K.E. New three component condensation in the presence of benzylidene acetophenones// Journal of Low Dimensional Systems, 2018, v.2, No2, p. 25-28

9. Maharramov A.M.,Ismiyev A.I.,Hajiyeva K.E. The study of antimicrobial activity of 2-amino-1-methyl-6-(methylthio)-5-nitro-4-aryl-1,4-dihydro-pyridine-3-carbonitriles// Journal of Low Dimensional Systems, 2018, v.2, No1, pp.45-47.

10. M. Xia, Chen Q., LuY.-D. Microwave-promoted synthesis of 2-amino-4-aryl-4H-pyrans on soluble polymeric support// Synth. Commun., 2005, v.35, No10, pp. 1381-1390.

11. Khurana J.M., Chaudhary A. Efficient and green synthesis of 4H-pyrans and 4H-pyrano[2,3-c] pyrazoles catalyzed by task-specific ionic liquid [bmim]OH under solvent-free conditions// Green Chemistry Letters and Reviews, 2012, v.5, No4, pp.633-638.

12. Elnagdi N.M. H., Al-Hokbany N. S.Organocatalysis in synthesis: L-proline as an enantioselective catalyst in the synthesis of pyrans and thiopyrans // Molecules, 2012, v.17, No4, pp.4300-4312.

13. El-Bayouki K. A. M., Basyouni W. M., Khatab T. K., El-Basyoni F.A. Efficient and expeditious synthesis of pyrano-pyrimidines, multi-substitutedγ-pyrans, and their antioxidant activity// J. Heterocyclic Chem., 2013, v.51, No1, pp.106-115.

14. Amirnejad M., Naimi-Jamal M. R., Tourani H., Ghafuri H. A facile sol-vent-free one-pot three-component method for the synthesis of 2 amino-4H-pyrans and tetrahydro-4H-chromenes at ambient temperature// MonatshChem, 2013, v.144, No 8, pp.1219–1225.

15. CuriniM., PreziusoF., Taddeo V.A., EpifanoF.Ytterbiumtriflate promoted solvent-free synthesis of 2-amino-4*H*-pyranes// Tetrahedron Letters, 2017, v.58, No16, pp.1659-1661.

16. Sheldrick G.M. SHELXTL Structure Determination Software Suite, Brüker AXS, Madison, Wisconsin, USA, 2008,v.6.12.

APPLICATION OF THE MODEL OF MANAGEMENT OF SOIL FERTILITY TO PRESERVE THE PRODUCTIVITY OF THE SOIL UNDER THE VINEYARDS

N.A.SADIGOVA[1], M.M.YUSIFOVA[1]*, N.A.SULTANOVA[2]

[1]Faculty of Ecology and Soil Science, Baku State University, Baku, Azerbaijan, AZ 1148, Z.Chalil. str.53.
[2]Baku Slavic University, Baku, Azerbaijan, S.Rustamstreet 33

Carrying out of the complex investigations according to the growing condition of the plants paying attention to their necessity for the environment, the structure and characters of the soils, increase of soil fertility and productivity of agrocenosis is one of the main problems.The investigation of composing the soil-plant-landscape system in order to learn the relation of it with the natural and anthropogenic factors has been carried out according to structural elements of ecological fertility model.

1. INTRODUCTION

V.A.Kovda shows in his monograph called "Biological systems in agriculture and forestry" that each private ecosystem - biogeocenosis is a historic formed self - regulating mechanism and represents a certain level of formation and mutual influence of animated object and dead matter. Biogeocenosis is formed from the plant, livings, microorganisms, homogenous soil surface and it is characterized by the mutual influence and depends of material and energetic exchange process.

The boundry of the spreading areals is determined by the border of phytocenosis. The human's influence on biogeocenosis by agriculture, forest and water economy requires the management of biosphere and its components in the scientific-grounded form. If the cognition of ecosystem is scientific and trustworthy, its management methods and technique is exact, tender and perfect then the obtaining product will be high.

At present the investigation of the complicated systems as biogeocenosis requires a construction of the conceptual model of the object studying by the application of the systematic method of approaching, so expressing its structure, functions and mutual relations by a word, graphic, formula and figures. One of the main methods is modelling for carrying out such investigations [1].

It is impossible to solve the increase of the productivity of soil and landscape by any method without the investigation of the complex methods. Soil is the most guided component being one of the main composition parts of biosphere in present developed level of the science and technique. The man can control water ecosystem and organisms a little (by the soil), but he can't intervene in atmosphere and climate.

So, it is necessary to possess the trusty scientific basis about the same soils for the solution of the problems of the control of soil fertility. The construction of the models of soil fertility in a different level gives an opportunity to form such bases on the basis of information methods [2]. It is necessary to take account that the laws of "Nature harmony" action in the natural landscapes, at this time the exchange of substance, energy and information is in the form of equivalent among the ecosystem components. The balance of this energy, substance and information is disordered for some or other direction under the influence of long anthropogenic in agrosystems.

We consider advisable to carry out the investigation of natural biogeocenosis (including, pasture biogeocenosis) over three rings connected with the hierarchical chain: soil – plant - landscape system. In this connection it is necessary to carry out the system

of investigations over its each composition part (object). The main object of the research is a soil, complex and open functional dynamic system and its structure, character and regimes must be investigated [3].

The second object – the plant (phytocenosis) possesses the ability of crop production being material carrier of the whole system. Here mainly the reaction of the plant to character and regimes of the soil is studied from a cropquality and quantity standpoint. The third object of the research is a landscape of the land (geological basis, soilforming rocks, land relief, climate, hydrothermic condition). Here the landscape is studied as a general background in hierarchic connection.

Thanks to I.I.Karmanov, D.S.Bulgakov [4], N.N.Rozov, D.S.Bulgakov, N.N.Vadkovskaya [5], L.L.Shishov, D.N.Durmanov, I.I.Karmanov [6,7], G.Sh.Mammadov's [8] methodical instructions we worked out the structure of ecological fertility model of the under vineyards soils taking account the noted characters of biogeocenosis under G.Sh.Mammadov's leadership.

2. RESULTSAND DISCUSSION

The ecological fertility model of under vineyards soils is a schematic structure formed from the blocks of the study of the complexity of the mutual relation with the natural and anthropogenic factors of the soil – plant - landscape system by the application of the system approach. The blocks are formed of the factors, elements and parameters reflecting the direction of the changes taking place as a result of natural process and anthropogenic influence.

The ecological fertility model of under vineyards soils is formed of 7 blocks differing for the importance, significance degree in fertility control: ecological block, soil composition, the block of soil characters, plant block, evaluation block, monitoring block, agromelioration block.

Ecological block is formed from two subblocks: climate and relief. The climate factors fix the space-atmosphere parameters in itself forming energy source of biogeocenosis (radiation, rainfalls, temperature,

evaporation, wind, humidity and etc). The intensity of the sun radiation determines the intensity of photosynthesis having influence on plant directly.

The rainfalls have influence on plant indirectly by the change of soil fertility. The air temperature has influence on intensity of biochemical process on the surface of the plant. The speed and direction of the wind condition turbulent process changing air temperature and wetness. The high speed of the wind is cause for deformation process and it has destroying influence on plant.
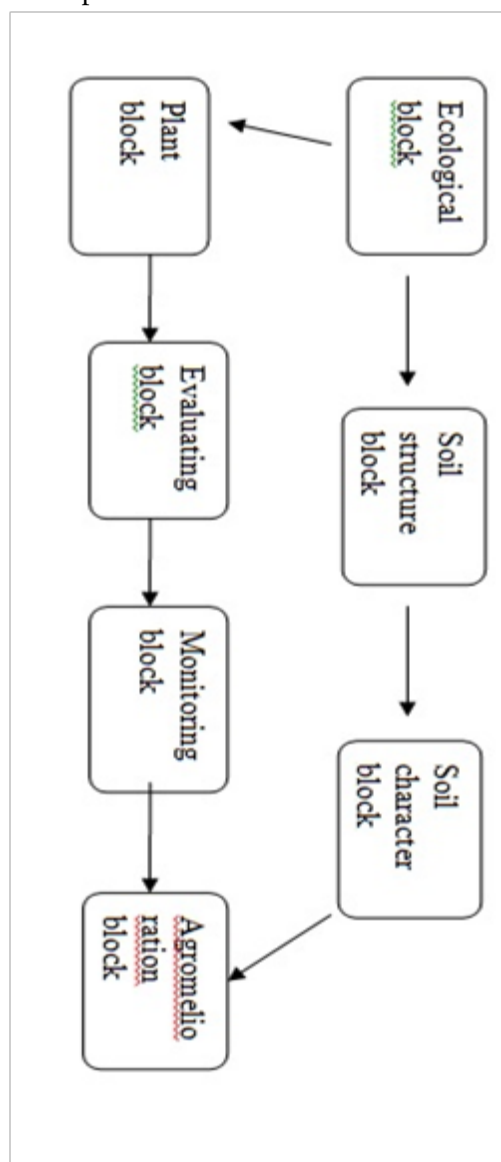

Figure 1 . Structural elements of the ecological fertility model

The relief sub block is formed from the following factors: relative and absolute height, the inclination of the slopes, level of subsoil waters, vertical and

horizontal distribution of air flow. Different kinds of relief soil has influence on settlement of natural plant cover, air-water regime of soils, mechanical composition, technological characters. Relief increases or decreases the intensity of the climate factors distributing them on the surface.

Thus the inclination of the slopes is the main factor which changes the intensity of sun radiation: the length and inclination of the slopes distribute rainfalls, the absolute height changes the composition of atmosphere and etc. The relief factors change the temperature of soil cover, condition the intensity of alluvial, delluvial, proluvial and eol deposits, erosion and deflation projection.

They are the blocks of gathering the character and parameters of soil which is the main component of biogeocenosis, of soil composition and characters informing about the factors limiting the fertility, and they play a leading role in structure of the ecological model. The soil cover offers facilities for photosynthetic activity of the plants providing the nutrition of the plants by mineral, water, carbon dioxide gas and nutrients.

V.A.Kovda writes that the soil represents the living environment and condition of plant, animal and microorganisms. The soil cover plays a role as a screen for preventing the stream of the important elements of biosphere into the world ocean and the geochemical stream to the deserts [4]. It fulfills universal, biological absorbent, destructive and neutralizing functions.

The soil has influence on plant by the activity and concentration of the biologically active substances and chemical elements on the horizon where the root spreads. The soil belongs to open systems as biogeocenosis, so they are not only in the substance and energy exchange between themselves, also between the neighboring systems.

The soil composition block is separated into three sub blocks: granulometric, organic and chemical composition. The granulometric composition possesses integral function in formation of agronomic characters of the soils, determines water, air and heat regimes of the soil, and it influences on intensity of the whole physiological and biological process of the plant.

The organic composition reflects the quantity of humus by percentage and its reserve. Humus plays an integrator role of soil fertility, gives an opportunity to define the possible directions of the increase of fertility, plays a leading role in formation of the valuable agronomic structure. Humus stimulates the growth and development of the soil having influence on it directly. The sum of the absorbing bases (by mg-ekv) and mineral biogenic elements – the quantity and reserve of nitrogen, phosphorus, potassium include in chemical structure (by %).

The block of soil characters gathers agro physical and agrochemical in itself.

One of the important structural parts of biogeocenosis is a plant, the plant produces biological mass, organic substance from unorganic matter assimilating energy and substance from the environment. The geobotanical information about the main fodder crops forming phytocenosis, association, plant types spread in the pastures investigating in a **plant block** is collected. The results of the analyses about biochemical composition of phytocenosis, the productivity over botanical - economic groups and general productivity of the plant formations, botanical sort composition and structure of the main plant are collected, the category, capacity, fitness degree of the pastures and the use norms of them are analyzed and determined.

The evaluating block. The evaluating block of under vineyards soils consists of composition parts as soil evaluate and grouping of agricultural - works, estimation of landscape complexes. The soil evaluate is a value of the comparative quantity of their fertility level. The main importance of the evaluate is a definition of the relation between soil characters and its productivity. During the evaluate the soil character is given by the constant parameters as a quantity of absorbed bases and nitrogen, phosphorus, potassium reserves. These parameters possess positive correlation by the plant productivity.

Agricultural - works grouping of the soils is generalization of soil units possessing similar and alike agronomic characters towards any plant or plant group. Such generalization is carried out obeying seriously to certain requires of soil condition. The

evaluate of the landscapes was carried out paying attention to important position of phytocenosis (plant association) in under vineyards soils. The landscape evaluate is the second stage after the soil evaluation and it gives a chance to evaluate the landscape complexes quantitatively differentiating qualitatively.

Monitoring block – ecological monitoring is such an observation system that the biosphere condition is studied, controlled, evaluated under the influence of natural and anthropogenic factors at a certain period and the future information is given. The ecological monitoring is separated into global, regional and local levels for generalization and capacity of the information. The negative changes happening in soil as a result of the influence of the anthropogenic pressure and natural factors necessitated the ecological control on soil, that is soil monitoring.

The superficial and solid improvement measures directed to the improvement of the rational use from under vineyards soils, water, air regime, soil composition are gathered in **agromelioration block.**

3. CONCLUSION

As agrobiogeocenosis (including the under vineyards soils) expose to transformation directing to degradation as a result of the human's advisable, plenty of time spontaneous activity protecting these ecosystems and rational using of them must be the main duty of the modeling. Models of soil fertility under the vineyards are made up of a 7 block, differing in the level of significance and importance.

4. REFERENCES

1. Agroecological model of soil fertility in Azerbaijan. Commentary information.Baku, AZETETII, 1993, p.78.
2. Mammadova S.Z. et al. Models of the fertility of soils useful for tea in Lenkoran region. Authoref.diss. cand.agric. Baku, 1989, p. 21

3. Laysk A.et al. /Aboutmodelling of productive process of the plant cover.Botanical journal, issue. 56, № 6, 1971, p.761-776
4. Karmanov I.I. et al. /Contemporary problems of the complex agronomic characteristics of soils.Soil Science, № 9, 1996, p.1119-1122.
5. Bulgakov D.S. et.al. / Prognosis of the increase of soil fertility on the basis of working out of agroecological models. Reports VASKHNIL, № 1, 1984, p.3-5
6. Shishov L.L. et.al. /Modelling of soil fertility. Problems of soil science, M., Science, 1990, p.78-83
7. Shishov L.L. et.al.Criterion and models of soil fertility, M., 1987, p.102
8. MammadovG.Sh. /Models of soil fertility in Azerbaijan SSR.Thesis of Resp. VII congr. of all-un. Assoc. Soil. №4, Tashkent, 1985, p. 194

PHOTOCATALYTIC SUBSTANCES IN ENVIRONMENTAL REMEDIATION

F.G. ALIYEV, S.A.HASANOVA*

Faculty of Ecology, Azerbaijan University of Architecture and Construction,

Az1073, 5 Ayna Sultanova St., Baku, Azerbaijan

In chemistry, photocatalysis is the acceleration of a photoreaction in the presence of a catalyst. In catalysed photolysis, light is absorbed by an adsorbed substrate. In photogenerated catalysis, the photocatalytic activity (PCA) depends on the ability of the catalyst to create electron–hole pairs, which generate free radicals (e.g. hydroxyl radicals: •OH) able to undergo secondary reactions. Its practical application was made possible by the discovery of water electrolysis by means of titanium dioxide (TiO_2).Metal oxides are of great technological importance in environmental remediation and electronics because of their capability to generate charge carriers when stimulated with required amount of energy. The promising arrangement of electronic structure, light absorption properties, and charge transport characteristics of most of the metal oxides has made possible its application as photocatalyst. In this article definition of metal oxides as photocatalyst, structural characteristics, requirements of the photocatalyst, classification of photocatalysts and the mechanism of the photocatalytic process are discussed.

1. INTRODUCTION

Photocatalysis, among all the various advanced oxidation processes is the one that has found wider use: it's a chemical reaction that mimics trees photosynthesis to absorb and transform pollutants into non-harmful elements.If we try to dig into details of this revolutionary discovery, we find that its operations follows just exactly what happens in nature. Photocatalysis imitates, as we said, the well-known photosynthesis in transforming harmful substances for mankind. The chemical process that is at the base is in fact an oxidation that starts thanks to the combined action of light (solar or artificial) and air.Photocatalysis is increasingly used as a method to clean up air and water, and the reasons why this process is becoming increasingly popular are the following:

o It significantly degrades recalcitrant pollutants present in the air and water

o The pollutant is mineralized to CO_2 and H_2O and not transferred into another phase

o It's cheap and does not require regeneration

o It's not selective, can eliminate lots of pollutants of different nature

o It takes advantage of UV light and water (in the case of air, humidity)

Photocatalysis is a science of employing catalyst that is utilized for speeding up chemical reactions that requires or engages light. A photocatalyst is defined as a material that is capable of absorbing light, producing electron–hole pairs that enable chemical transformations of the reaction participants and regenerate its chemical composition after each cycle of such interactions [1], [2], [3], [4], [5], [6]. There are two types of photocatalytic reactions i.e. homogeneous photocatalysis and heterogeneous photocatalysis.

The significant features of the photocatalytic system are the desired band gap, suitable morphology, high surface area, stability and reusability [3], [4], [5], [6]. Metal oxides such as oxides of vanadium, chromium, titanium, zinc, tin, and cerium having these characteristics follow similar primary photocatalytic processes such as light absorption, which induces a charge separation process with the formation of positive holes that are able to oxidize organic

substrates [4], [5], [6]. In this process, a metal oxide is activated with either UV light, visible light or a combination of both, and photoexcited electrons are promoted from the valence band to the conduction band, forming an electron/hole pair (e-/h+). The photogenerated pair (e-/h+) is able to reduce and/or oxidize a compound adsorbed on the photocatalyst surface. The photocatalytic activity of metal oxide comes from two sources: (i) generation of $\cdot$OH radicals by oxidation of OH^- anions, (ii) generation of O_2^- radicals by reduction of O_2. Both the radicals and anions can react with pollutants to degrade or otherwise transform them to lesser harmful byproducts [5], [6].

There are many catalysts reported in the literature for this exciting process. Among these metal oxides (TiO_2, ZnO, SnO_2 and CeO_2), which are abundant in nature, have also been extensively used as photocatalysts, particularly as heterogeneous photocatalyst since several decades [5], [6]. This is because of their biocompatibility, exceptional stability in a variety of conditions and capability to generate charge carriers when stimulated with required amount of light energy. The favourable combination of electronic structure, light absorption properties, charge transport characteristics and excited lifetimes of metal oxides has made it possible for their application as photocatalyst [2], [3], [4], [5], [6].

Heterogeneous photocatalysis employing metal oxides such as TiO_2, ZnO, SnO_2 and CeO_2 has proved its efficiency in degrading a wide range of distinct pollutants into biodegradable compounds and eventually mineralizing them to harmless carbon dioxide and water.

Recent research has also shown that (Fig. 1) metal oxides can be used as a photocatalyst to decompose toxic organic compounds, photovoltaics, prevent fogging of glass and even split water into hydrogen and oxygen [2], [3], [4], [5], [6]. Hence, they are of great technological importance in areas of environmental remediation, storage, hydrogen production and electronic industries [3], [4], [5], [6]. The heterogeneous photocatalysis is also being actively investigated (Fig. 1) as a promising self-cleaning, antibacterial and deodorization

system [3], [4], [5], [6]. The applications of such photocatalytic process are mostly needed for thepurification of waste water, by removal of bacteria and other pollutants, as this can render water reusable.

Figure 1. Possible applications of metal oxides

2. COMPARING PHOTOCATALYSTS

Among the photocatalysts, TiO2 is the one who found more use so far:
- It's a crystalline white powder
- Particularly effective if irradiated by UV rays
- Economic
- Very efficient in photocatalytic processes
- It's used as a colorant (E171) for different products (e.g. foodstuffs, toothpastes, paints), and it is therefore available in large quantities.

Titanium dioxide can exist in amorphous form or in three different crystalline forms: Rutile, tetragonal shape. It is the form used industrially. It may present a black color, reddish brown in larger crystals, or yellow in finer crystals.

Symmetry rhombic bipyramidalbrookite. In nature it's present in the form of very small flattened tubular crystals ranging in color from pink to brown

Anatase in distorted tetragonal form. It's the most stable polymorph at low values of pressure and temperature. It's the more active form catalytically speaking. The anatase Is in the form of small isolated crystals having a color ranging from blue to yellow (they all are octahedral structures (Ti06) where Ti has coordination number 6).

Among the photocatalysts, TiO_2 is the one who found more use so far:
- It's a crystalline white powder

o   Particularly effective if irradiated by UV rays

o   Economic

o   Very efficient in photocatalytic processes

o   It's used as a colorant (E171) for different products (e.g. foodstuffs, toothpastes, paints), and it is therefore available in large quantities.

Titanium dioxide can exist in amorphous form or in three different crystalline forms:

o   Rutile, tetragonal shape. It is the form used industrially. It may present a black color, reddish brown in larger crystals, or yellow in finer crystals Symmetry rhombic bipyramidalbrookite. In nature it's present in the form of very small flattened tubular crystals ranging in color from pink to brown

o   Anatase in distorted tetragonal form. It's the most stable polymorph at low values of pressure and temperature. It's the more active form catalytically speaking. The anatase Is in the form of small isolated crystals having a color ranging from blue to yellow (they all are octahedral structures (TiO_6) where Ti has coordination number 6).

There are several materials that show photocatalytical properties (TiO_2, ZnO, SnO_2, CdS, etc.), however not all are quite efficient and stable over time to be used for this purpose. This is because the ability to transfer the charge of a semiconductor is governed by the position of its band and by the potential of oxidation-reduction.

The oxidation-reduction potential is a measure of the tendency of a chemical species to acquire electrons, that is, to be reduced. Between two species that interact with each other: the species with lower potential E oxidizes (yields electrons) the species with higher potential E reduces (acquires electrons)

The red-ox potential of the hole in the valence band must be sufficiently positive to allow the acceptor function. The red-ox potential of e- in the conduction band must be sufficiently negative to allow the donor function. Otherphotocatalysts (like GaP, GaAs, CdSe, CdS or Fe_2O_3) appear to be less stable in air and to degrade more easily: ZnO, despite having a band gap width that lends itself well to promote the photocatalytic degradation processes of organic compounds in aqueous solution, forms a passivating

layer of $Zn(OH)_2$ on its surface which seriously compromises the characteristics

o SnO_2 has an excessively high band gap

o WO_3 tungsten trioxide instead is an excellent photocatalyst

Titanium dioxide is without doubt the photocatalyst that, for many reasons, find more uses from a commercial point of view; its limit is the fact that it is activated only under UV rays illumination, and this is a problem in case of a low percentage solar energy. For this reason, to overcome this limitation, our company has used a sensible catalyst to visible light also, such as tungsten trioxide.

3. PHOTOCATALYSIS BENEFITS

Now that we've understood the operations of photocatalysis, we can list its advantages. The photocatalytic process really brings the occurrence of three realities:

1. Antipollution
2. Antifouling
3. Antibacterial

These properties are simply the result of oxidation of substances that encounter a photocatalytic surface. If they are pollutants (nitrogen dioxide, sulfur dioxide, carbon monoxide, fine particulate matter) we can speak of antipollution reaction, if they are fouling substances (carbon blacks, dyes) we can talk about self-cleaning reaction, if they are bacteria, molds, fungi and microorganisms, we can speak of antibacterial reaction. Nowadays there is a long series of products using the concept of photocatalysis to improve the environment where we live, and at the same time to be compatible with the needs and style of the modern world.
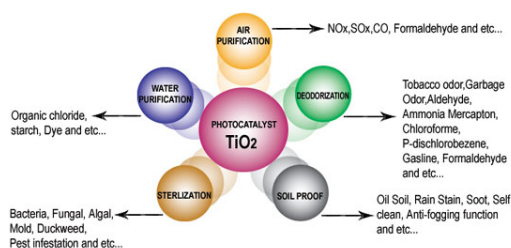

Figure 2. Benefits of photocatlyst TiO_2

The photocatalytic process is used in various engineering applications, which is whymany companies in the construction and air/water treatment industry are investing in this green technology.Without doubt the photocatalytic process, in the next few years, will play an increasingly important role in sustainable treatment processes.There are many products that could potentially be included in the daily use and that would give significant benefits to improve the air we breathe (e.g.: tiles with photocatalytic surface, photocatalytic cement and paints, water purification plants).

4. REFERENCES

1. S.H.S. Chan, T.Y. Wu, J.C. Juan, C.Y. The Recent developments of metal oxide semiconductors as photocatalysts in advanced oxidation processes (AOPs) for treatment of dye waste-water/J. Chem. Technol. Biotechnol., 86 (2011), pp. 1130-1158

2. Ibrahimova S., Aliyev F.G. et al. / Chemical Engineering Transactions, 200,v.47, p.199-204

3. E. Pelizzetti, C. Minero. Metal oxides as photocatalysts for environmental detoxificationComments Inorg. Chem., 15 (1994), pp. 297-337Marco Altomare, Gian

4. Luca Chiarello, Maria VittoriaDozzi, AlessiaSaccomanni,ElenaSelli. "Photocatalytic Hydrogen Production from Aqueous Solutions on Noble Metal-Modified and/or Doped TiO2".XXIV CongressoNazionaledellaSocietàChimicaItaliana.

Lecce, 11–16 September 2011. eISBN: 978-88-8305-085-5.

5. M.R. Hoffmann, S.T. Martin, W. Choi, D.W. Bah nemnEnvironmental applications of semiconductor photocatalysisChem. Rev., 95 (1995), pp. 69-96

6. H. Chen, C.E. Nanayakkara, V.H. GrassianTitanium dioxide photocatalysis in atmospheric chemistryChem. Rev., 112 (2012), pp. 5919-5948

7. H.K.Hhalilova,S.A.Hasanova,F.G.Aliyev.Photocatalytic Removal of Organic Pollutants from Industrial Wastewater Using TiO_2 Catalyst. Journal of Environmental Protection,2018,9, 691-698.

8. M. Pelaez, N.T. Nolan, S.C. Pillai, M.K. Seery, P. Falaras, A.G. Kontos, P.S.M.Dunlop, J.W.J. Hamilton, J.AByrne, K. O'Sheaf, M.H. Entezari, D.D. DionysiouAreview on thevisible light active titanium dioxide photocatalysts for environmental applicationsAppl. Catal. B, 125 (2012), pp. 331-349

9. M. V. Dozzi, G. L. Chiarello and E. Selli, J. Adv. Oxid. "Effects of Surface Modification on the Photocatalytic Activity of TiO2". Technol., 2010, 13, 305–312.

Journal of LDS